Joonas Kivi

Algorithmic road state modelling

School of Science

Thesis submitted for examination for the degree of Master of Science in Technology.

Espoo 26.9.2019

Thesis supervisor:

Prof. Antti Hannukainen

Thesis advisor:

M.Sc. (Tech.) Kimmo Kynnös

Aalto University
School of Science

AALTO UNIVERSITY
SCHOOL OF SCIENCE

ABSTRACT OF THE
MASTER'S THESIS

Author: Joonas Kivi

Title: Algorithmic road state modelling

Date: 26.9.2019 Language: English Number of pages: 6+55

Department of Mathematics and Systems Analysis

Professorship: Applied Mathematics Code: SCI3053

Supervisor: Prof. Antti Hannukainen

Advisor: M.Sc. (Tech.) Kimmo Kynnös

In this work we aim to present algorithms for determining the depth of water or thickness of ice on the road surface from the short-wave infrared absorption spectra of the layer for a Vaisala mobile road sensor prototype.
First we build a general understanding of the measurement situation and present a novel, reliable method for the reference measurement of both water and ice layers. Finally, we present two potential algorithms. The first one is based on a rudimentary physical model of the measurement situation while the second features a more data-driven approach. The performance of both of these algorithms is benchmarked against a baseline algorithm. The data-driven approach produces most promising results, as it leverages well the extensive reference measurement.

Keywords: Road weather, Absorption Spectroscopy, Pavement Surface

AALTO-YLIOPISTO
PERUSTIETEIDEN KORKEAKOULU

DIPLOMITYÖN
TIIVISTELMÄ

Tekijä: Joonas Kivi

Työn nimi: Algoritminen tienpinnan tilan mallinnus

Päivämäärä: 26.9.2019 Kieli: Englanti Sivumäärä: 6+55

Matematiikan ja systeemianalyysin laitos

Professuuri: Sovellettu matematiikka Koodi: SCI3053

Valvoja: Prof. Antti Hannukainen

Ohjaaja: DI Kimmo Kynnös

Tämän työn tavoitteena on kehittää algoritmeja tienpinnalla olevien vesi- ja jääkerrosten paksuuden määrittämiseksi näiden lähi-infrapuna-alueen absorptiospektrejä mittaamalla. Algoritmien toimintaa testataan Vaisalan kehittämällä tiesääanturiprototyypillä.

Käymme ensin läpi kerrospaksuuksien mittaamisen perusteet ja mittaustilanteen yleisellä tasolla. Esittelemme myös uuden, tarkan referenssimittausmeneltelmän kontrolloitujen vesi- ja jääkerrosten luomiseen ja mittaamiseen laboratorio-olosuhteissa.

Lopuksi esittelemme kaksi ehdokasta kerrospaksuusalgoritmiksi. Ensimmäinen näistä perustuu alkeelliseen fysikaaliseen malliin mittaustilanteesta kun taas toisessa on datalähtöisempi lähestymistapa. Datalähtöinen menetelmä tuottaa lopulta lupaavimpia tuloksia, koska se pystyy hyödyntämään tehokkaasti uuden referenssimittauksen tuloksia.

Avainsanat: Tiesää, Spektroskopia, Asfaltti

Preface

I wrote this thesis while employed at Vaisala Oyj. and the work was largely motivated by furthering the development of the Vaisala mobile road weather sensor, launched earlier this year. The contents of this work thus reflect a slice of the breadth of the questions that arose during the product development process.

I also wanted to write a thorough and uncomplicated overview of the basics of both the measurement method and situation. The background section is designed with this in mind, with allegorical examples, plentiful illustrative pictures and a physical explanation from the very basic principles of absorption. I hope the content proves valuable to both customers and future Vaisala employees.

The development of both the sensor and the field in general will continue well past this work and I'm enthusiastic to continue my work both with sensor and the team behind it.

I would like to offer my heartfelt thanks to Antti Hannukainen, the supervisor of this thesis, who offered very active and helpful supervision. Equally I offer my thanks to my thesis advisor Kimmo Kynnös and my other colleagues at Vaisala. Finally, my thanks go to my beloved Mariia, my friends, and family for their support and patience during the writing of this thesis.

Otaniemi, 26.9.2019

Joonas Kivi

Contents

1 Introduction

Accurate road weather information is integral to the design, planning and execution of effective road safety measures: maintenance, deicing, warning systems and situational speed limits. In general, accurate weather information plays a part in saving both lives and on costs through smarter allocation of road safety resources.

In this work we discuss methods for accurate water and ice layer measurement in road weather context, specifically studying the Vaisala mobile road weather sensor prototype. Simply put: we want to measure from a moving car and determine whether there is water or ice on the road, and how much. We identify and quantify the main sources of uncertainty of the measurement. Lastly, we present and compare different algorithms for approximating the amount of water and ice in relation to the uncertainties discussed.

1.1 Mobile road sensor prototype MORSE

The prototype sensor studied is informally called MORSE, as in Mobile Road Sensor. The device is presented in Figure 1. For brevity we will use this unofficial moniker instead of referring to the sensor as the mobile road sensor prototype each time.

The Vaisala MORSE is a mobile remote road state sensor. It determines the amount of water or ice on the road surface for winter maintenance and grip approximation purposes. It uses three-wavelength laser spectroscopy to measure the absorption spectrum of the layer covering the road. The approximate thickness is then derived from the absorption spectrum. This process requires a layer thickness model: a function that describes the connection between spectral changes and amount of water and ice. MORSE also features complementary measurements on air temperature, humidity and road surface temperature for determining the most likely layer thicknesses.

MORSE uses the same basic technology and modelling as Vaisala's stationary remote road state sensor DSC-211 [19], comparing the spectra of wet road surfaces with a known dry spectrum, and calculating the layer thickness from their difference. Accounting for the new challenges and possibilities of mobile measurement with new iterations of the modelling algorithm is the main aim of this thesis.

1.2 More accurate mobile water and ice measurement

The focus of this thesis is to increase the measurement capability of the MORSE, allowing more accurate layer thickness information in mobile measurement context. There are two main applications for layer thickness information in the context of road weather: winter maintenance and friction approximation.

In winter maintenance information on water and ice amounts is useful for spreading salt and other deicing chemicals. Road salt is both expensive and harmful to the environment. Information on the amount of water or ice on the road allows more exact salt dispensing, leading to notable savings in road maintenance [12].

Figure 1: The mobile road sensor prototype MORSE. The three adjacent lenses are for the three lasers used and the larger one below them is for the receiver. On the upper left side is the surface temperature sensor and on the right a humidity and temperature probe.

There is also a clear consensus on the effect of rainfall on accidents: wet roads cause crashes, largely due to the loss of friction from water on the road [17]. More accurate friction approximation, achieved through more accurate water layer thickness readings, would thus help prevent loss of life in these cases through either cautioning the drivers or automatically lowering the speed limit accordingly. This could also lead to the possibility of increasing the speed limits under good driving conditions.

A great need for both sensors such as the MORSE and general technical study concerning the subject is evident, as the field is in rapid development, calling for solutions to the issues hindering the adoption of vehicle-based weather measurements [9].

1.3 Surface structure measurement

The "effective layer thickness" is different for both of the mentioned applications. Water layer thickness can be defined in different ways. We conjecture that the different definitions can be linked using general information on the road surface, specifically height distribution. The praxis of this is however more challenging, as

accounting for the surface structure necessitates somewhat accurate measurement thereof.

Linking the different definitions together would allow us to provide useful information for separate applications. Surface structure information would also be useful in its own right, providing valuable data for road maintenance. Thus studying methods of characterising the height distribution is an important auxiliary goal for general mobile measurement improvement.

2 Background

2.1 Principle of operation

The laser spectroscopy employed by the MORSE sensor relies on spectral changes due to water and ice coverage in the short wave infrared (SW-IR) range. Water and ice layers absorb distinct select wavelengths while allowing others pass through unimpeded.

2.1.1 Allegorical explanation

A helpful allegory to laser spectroscopy layer thickness measurement is that of the thickness of translucent coloured liquid, e.g. red wine in a glass. A thin layer of red wine, observable in a glass almost empty, is quite translucent and only slightly tinting. A layer of medium thickness is still somewhat transparent but highly tinting: one can discern shapes and brighter and darker areas, but no colour other than red. A thick layer is essentially opaque: all light regardless of colour is extinct, making the centre of a full glass of wine dark. This effect is illustrated in Figure 2. Wine absorbed into a porous surface, e.g. a tablecloth, will similarly alter the colour of the surface.

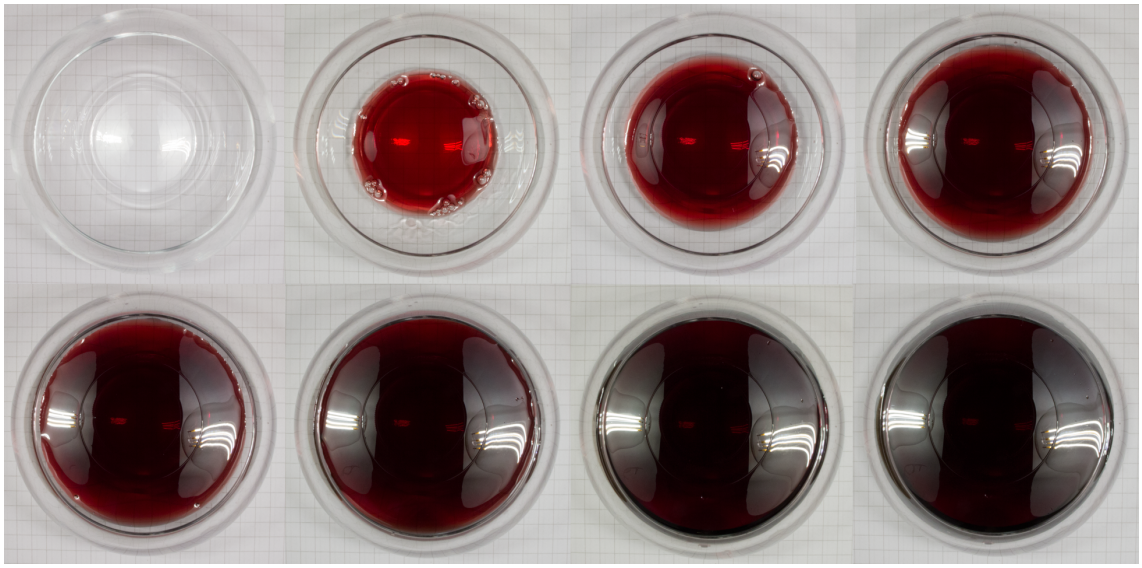

Figure 2: As the layer of wine thickens, the tint first becomes increasingly red, then dark.

A human observer can somewhat accurately approximate the thickness of wine layers by these changes in tint and translucency. Similarly, the MORSE observes colour changes on the surface, but in the short-wave infrared range, invisible to human eyes. In the SW-IR range water is translucent, like wine in visible wavelengths. Darker, more tinted values hint to higher layer thicknesses, the principle remains the same.

The three wavelengths used by the sensor can be compared to the cone cells of the human eye: the human eye can observe red, green, and blue, and deduce the combination thereof from the relative brightness of each colour, coming to an approximation of the thickness of the wine layer. Given another, blue liquid one could easily differentiate between the two and even try to approximate the mix ratio of the coloured liquids. Analogously, the three colours observed by MORSE allow it to deduce the amount of water or ice.

2.1.2 Physical explanation

In this section we formulate a simple physical model for spectroscopy measurement. This also functions as a simple physical explanation of the sensor measurement.

A beam of light travelling in a medium constantly loses intensity. A medium's ability to transfer light is called transmittance, and defined as the ratio between the intensities sent and received, i.e.

$$T = \frac{I_r}{I_s}, \tag{1}$$

where I_s is the original intensity, and I_r the intensity after passing through the medium.

This process is described by the Beer-Lambert law: the absorption of light into a medium is dependent on the path length and concentration of absorptive elements in the medium. For transmittance T is holds that

$$T = e^{-\Sigma_{i=1}^{N} \sigma_i \int_0^l \hat{n}_i(z)dz}, \tag{2}$$

where N is the number of different absorbent media, l is the path length of the optical beam, and σ_i and $\hat{n}_i$ are attenuation cross-section and number density, quantities describing the absorption rate of a thin layer of the medium. Number density is simply the number of molecules per volume, i.e. $\hat{n} = \frac{N}{V}$. It is not to be confused with the refractive index, which we will be discussing later. Attenuation cross-section σ is the effective cross-section of one molecule, the area through which a photon may not pass without being absorbed or scattered. Conversely any photons passing a molecule outside its attenuation cross-section will not be affected by the molecule. By multiplying number density and attenuation cross-section we arrive at the average relative area covered by the absorbent molecules per volume. This quantity is more commonly known as the attenuation coefficient.

The integral notation is useful for operating with multiple layers. Consider a medium consisting of two absorbent layers, air and water, and a reflective surface, the pavement. The beam of light travels through the absorptive layers, is reflected off of the pavement, scattered, and partially travels back through the same absorptive layers before being registered by the sensor. This process is illustrated in Figure 3.

The absorption-reflection process consists of three distinct phases: absorption before reflection, the reflection itself, and the absorption after reflection. Assuming that the two layers are homogeneous and separate,

$$\int_0^l \hat{n}_i(z)dz = l_i\hat{n}_i, \text{ for } i = 1, 2 \tag{3}$$

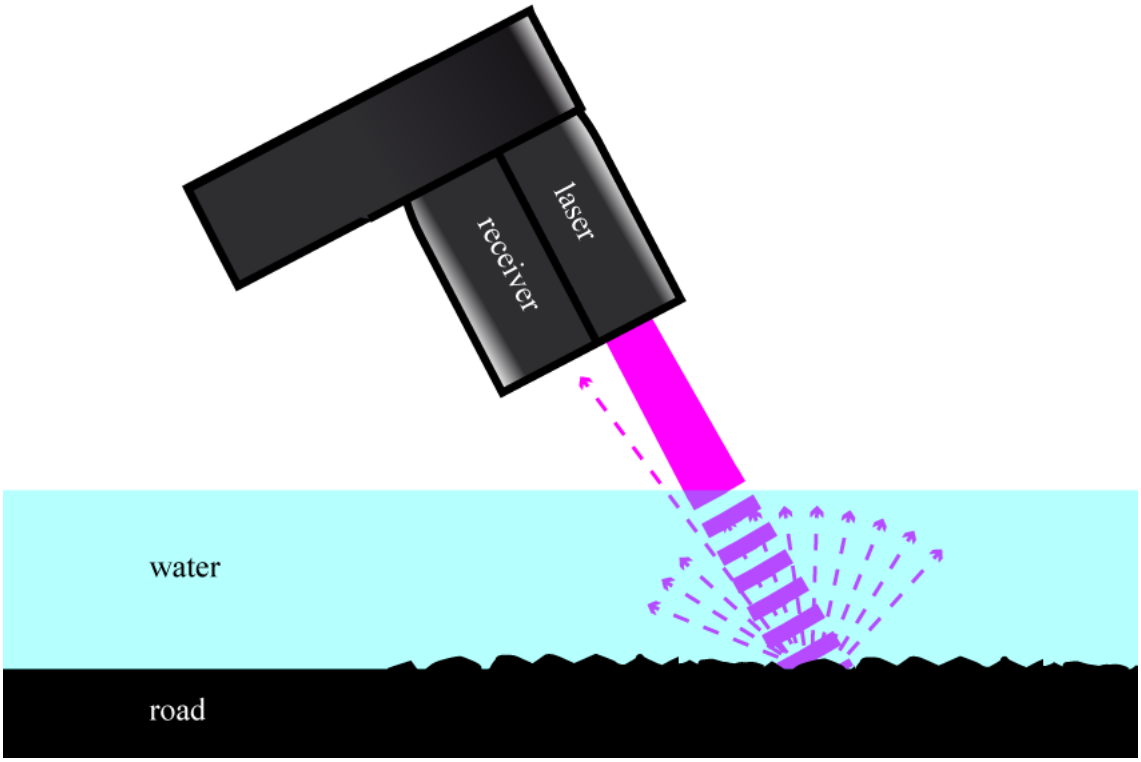

Figure 3: The sensor produces a laser beam, which is partially absorbed by the medium, reflected off of the pavement, and then received by the sensor.

where l_1 and l_2 are the distances travelled by the beam in air and water, respectively. Naturally then $l = l_1 + l_2$.

To sum up the three-step-process of transmittance, reflection and transmittance, the intensity received by the sensor now follows

$$I_r = I_s T_1 R T_2, \tag{4}$$

where I_s is the original intensity of the beam, T_1 is the sensor-to-road transmittance, R is the diffuse reflection, and T_2 is the road-to-sensor transmittance. Let's assume R to be constant for now. For this simplified model of transmittance $T_1 = T_2$, so we arrive at

$$I_r = I_s R T^2, \tag{5}$$

By combining Equation (5) with the Beer-Lambert law from Equation (2), we arrive at

$$I_r = I_s R e^{-2(\sigma_a \hat{n}_a l_a + \sigma_w \hat{n}_w l_w)}, \tag{6}$$

where the index a refers to air and w to water. Since $l_a \gg l_w$ we assume it constant in relation to l_w with minimal error: there is no significant change in the absorption of the air layer, even though it may be shortened by several millimetres. Now we can regroup and combine all the values constant in relation to l_w into a single term.

$$I_r = \underbrace{I_s R e^{-2\sigma_a \hat{n}_a l_a}}_{I_0} e^{-2\sigma_w \hat{n}_w l_w} \tag{7}$$

For a dry surface with $l_w = 0$,

$$I_r = I_s R e^{-2\sigma_a \hat{n}_a l_a} = I_0 \tag{8}$$

We will refer to this original intensity with no water as I_0. Furthermore, for now it will be assumed to be a known constant: we will measure the *dry reference* before measuring water layers. We likewise replace $\sigma_w n_w$ with extinction coefficient κ and remove the now unnecessary indexing to arrive at a fairly simple formula describing the measurement situation

$$I = I_0 e^{-2l\kappa}. \tag{9}$$

We use the dry signal values I_0 as a reference and are then able to approximate optical path length l from relative received signal intensity, as the Equation (9) can be solved as

$$l = -\frac{1}{2\kappa} \ln(\frac{I}{I_0}). \tag{10}$$

To derive water layer thickness from beam path length, one needs still correct for the measurement geometry and refraction of light. This is discussed in Section 2.2.4, more specifically Equation (15). For a steady measurement angle this is however a rather simple constant correction coefficient.

In relation to the previously discussed allegorical overview of the measurement, uniform absorption and optical path length relate to the opacity of the sample: the thicker the layer, the darker and more opaque it is.

2.1.3 Spectral dependence

While optical path length explains the opacity, spectral dependence represents the tinting effect. The extinction coefficient κ is dependent on the medium material and beam wavelength, i.e. $\kappa = \kappa(m, \lambda)$. This is equivalent to different materials having different colours in the visible spectrum. Spectrometry employs this dependency to differentiate between different states of matter and their respective layer thicknesses.

Measurement of at least two different wavelengths is required in order to differentiate water and ice from one another. In Figure 4 one can observe the extinction coefficient spectra of liquid water and ice. Beer-Lambert law assumes that the different media act independently of one another, so applying the previous layer-wise uniform version of Beer-Lambert for two lasers with different wavelengths and known initial intensities and material specific extinction coefficients we would arrive at

$$\begin{cases} I_1 = I_{01} e^{-2l_1 \kappa(m_1, \lambda_1)} e^{-2l_2 \kappa(m_2, \lambda_1)} \\ I_2 = I_{02} e^{-2l_2 \kappa(m_2, \lambda_2)} e^{-2l_1 \kappa(m_1, \lambda_2)}. \end{cases} \tag{11}$$

Naturally $l_i \geq 0$ for both materials. Given two equations with two unknowns, one can solve this pair of equations to determine the optical path lengths l_1 and

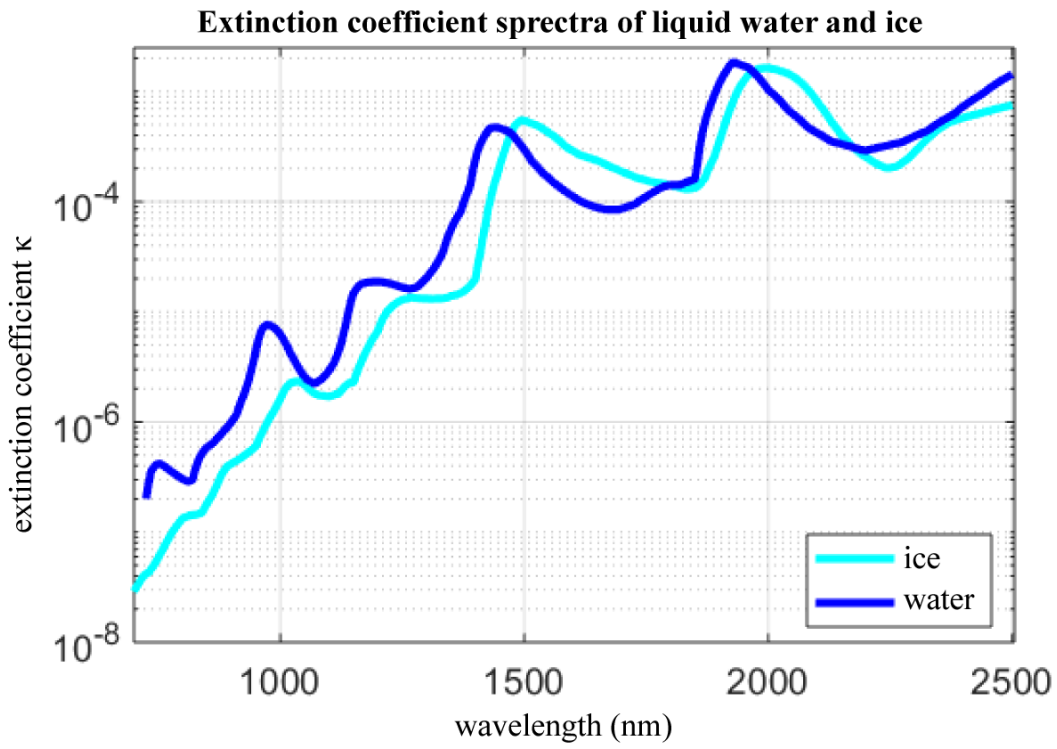

Figure 4: Extinction spectra of water (blue) and ice (cyan) in the SW-IR-region, data from Palmer and Williams [13], and Warren and Brandt [23], respectively.

l_2 for both materials, similarly to the solved form in Equation (10). In theory, the optical path length can be computed for both mediums and any mixture thereof.

In practice one faces several complications to this simple model. By selecting wavelengths λ_1 and λ_2 with strong spectral differentiation between ice and water we increase our signal-to-noise ratio, when considering our ability to measure the respective thicknesses of the media. A higher extinction coefficient in turn increases the magnitude of the measured effect. Thus e.g. λ_1 =1400 nm and λ_2 =1500 nm could be from prima principia considered suitable choices of wavelengths for the measurement. Both good differentiation and high absorption are required for the robustness of the measurement in more challenging conditions.

2.2 Uncertainty and complications

There are several factors that limit the viability of the spectroscopy employed. Some complications need to be taken into account and ultimately we are still left with uncertainties we have to account for in a more heuristic manner. Many of these complications hold for both the stationary and mobile measurement environments.

2.2.1 Intensity noise and spectral noise

We divide the measurement noise into intensity noise and spectral noise. The division is artificial but useful, as we will see in later sections.

The intensity mostly varies discretely when in motion, as the sensor measures different pavement types: it is first and foremost a consequence of the mobile measurement setup. When stationary the noise is negligible for all but layers closer to 10 mm in thickness.

Here we define intensity error or intensity noise as considered uniform decrease or increase in (the average of) signal levels I_i. For the mobile measurement it is caused especially by varying pavement qualities, and the effect is quite large. It can be modelled with uniform scalar multiplication of the signal levels I_i.

Spectral error, by contrast, is then the opposite of uniform intensity error: the average intensity stays the same, but the signal values are altered in relation to one another. Spectral error is introduced by the changing pavement colour and by pavement structure.

Using α for the uniform intensity error and γ_i for the spectral error, we arrive at

$$\begin{cases} I_1 = \alpha\gamma_1 I_{01} e^{-2l_1\kappa(m_1,\lambda_1)} e^{-2l_2\kappa(m_2,\lambda_1)} \\ I_2 = \alpha\gamma_2 I_{02} e^{-2l_2\kappa(m_2,\lambda_2)} e^{-2l_1\kappa(m_1,\lambda_2)} \\ \qquad\qquad\qquad \dfrac{\gamma_1 + \gamma_2}{2} = 1. \end{cases} \tag{12}$$

In the later equations describing the physics of the model we will forego these error terms, as they complicate the system of equations.

As an outline, intensity errors are much more common and prevalent. Even quadrupled changes in signal levels have been observed in measurement situations due to different contaminants and changing measurement surfaces. Spectral errors are rarer and smaller in magnitude, but require more understanding and better heuristics to account for.

2.2.2 Contaminants and a third laser

The water layer atop of the road often contains different contaminants, such as dust particles and decayed foliage. They may cause a rise in signal levels due to increased reflection or decrease due to absorption. Similarly airborne dust could theoretically interfere with the measurement, scattering the light in unwanted ways.

The MORSE sensor features a third laser with a wavelength roughly equally absorbent in both water and ice, e.g. λ_3 =1050 nm as one can observe in Figure 4. This results in four equations with three unknown path lengths l_i, adding an additional equation, thus giving leeway for managing uncertainty.

$$\begin{cases} I_1 = I_{01}e^{-2l_1\kappa(m_1,\lambda_1)}e^{-2l_2\kappa(m_2,\lambda_1)} \\ I_2 = I_{02}e^{-2l_2\kappa(m_2,\lambda_2)}e^{-2l_1\kappa(m_1,\lambda_2)} \\ I_3 = I_{03}e^{-2l_3\kappa(m,\lambda_3)} \\ l_3 = l_2 + l_1 \end{cases} \tag{13}$$

Apparently original design intent was to include the third laser to account for the uniform intensity error caused by the different contaminants inside the water layer, but his third wavelength can be useful in a multitude of ways. This additional information sets us free from the dependence on absolute signal values I_i and to study the relative values $\frac{I_i}{I_3}$ as a simple first solution to intensity error. This method would ignore e.g. dust that affects all three wavelengths roughly equally. Since the wavelengths have been chosen for strong differentiation of water and ice, most contaminants feature relatively little spectrum, so this simple method can mitigate their effect to a great length.

2.2.3 Wetting induced reflectance decrease

Porous materials turn darker when wet, and pavement surface is no exception to this, as we see in Figure 5. This phenomenon is caused by decreased reflectance on the water-to-matter surface and it is a phenomenon separate from the absorption of the medium. See [7] for a thorough discussion on this subject: there are other phenomena affecting the darkness in addition to the one discussed here. The phenomenon is useful for differentiating between dry and moist road surfaces when studying the absolute signal values, but ultimately troublesome for our measurement.

In its simplest form reflectance decrease due to wetting is described by the Fresnel equations. Since we are only interested in light reflected back to the sensor, we may assume normal incidence on the micro-level. This allows us to use the simplified form of the Fresnel equation, stating the reflectance R as

$$R = \left| \frac{n_1 - n_2}{n_1 + n_2} \right|^2 . \tag{14}$$

From the Equation (14) one can observe that the closer the two surfaces are in refractive index, the lower a reflectance we should expect. By plugging in $n_2 = 1.65$ for pavement [8] and alternative n_1's of 1 and 1.3 for air and water respectively, we arrive at a theoretical relative signal level decrease of approximately 75% between dry and wet bitumen. In laboratory tests we observed typically a 65% decrease in signal levels before the absorption becomes the dominant effect, so the observations are in rough agreement with the theoretical values. These however depend strongly on the surface observed: for less bituminous, older pavements with lower refractive indices we would expect higher relative signal level decreases according to this theory, due to lower refractive indices.

Wetting causes a considerable change in reflectance R and while dry intensities I_0 as presented in Equation (7) and presumed constant. Thus a separate variable for

Figure 5: Example of wetting: piece of pavement half wet.

wetting should be introduced. The differences in the refractive spectrum of water (opposed to the absorptive) are relatively small, but still large enough to occasionally produce gross measurement error together with other error sources. However, we will consider the effect as uniform intensity error for simplicity.

The spectral effect is mitigated by the absorptive index: in general in the SW-IR area, higher wavelengths correspond to slightly lower refractive indices [3] and to higher general absorption, as previously visible in Figure 4. This is both a blessing and a curse: while it makes the quantification of the wetting effect hard, it also mitigates the spectral error induced by ignoring it.

2.2.4 Angular dependency

To our knowledge, there are three angle dependent phenomena that affect our measurement: refracted geometrical pencil length, polarised reflection effects, and direct reflection from the water surface.

Direct reflection is a considerable effect only at very acute incident angles, and thus easily avoided. At those acute angles the reflection from the water surface would dominate the observed signal, making accurate absorption measurement impossible. That is why we opt to measure at less acute incident angles, even though we will

have to account for the more complex geometry.

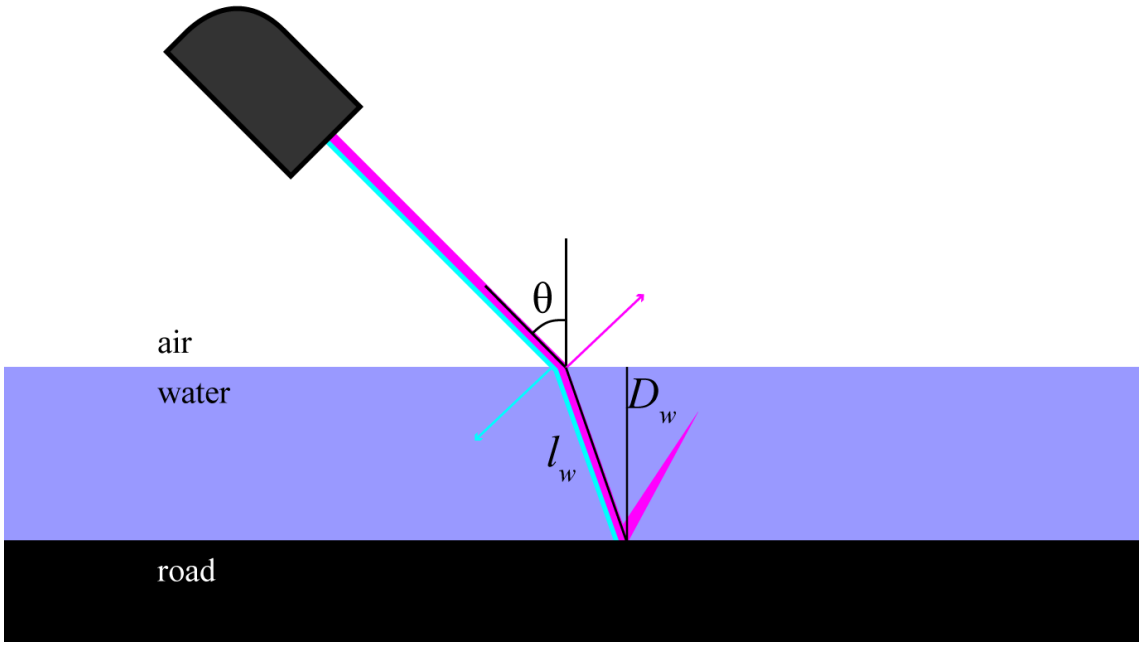

Figure 6: Illustration of the measurement refraction geometry. The laser beam projected (magenta) by the MORSE at angle of incidence θ is refracted by the water, then partially reflected back (cyan) by the pavement surface. Most of the signal is lost at the water-pavement interface due to absorption and diffuse reflection. Further losses are induced at air-water and water-air interfaces by reflections. All of these effects are dependent on the measurement angle. The effect of refraction is exaggerated for clarity.

The angle at which the pencil of light enters the water naturally affects the distance it travels therein. At more obtuse incident angles the distance travelled is longer, simply due to the reflection geometry. The distance is further affected by the refraction of light. This phenomenon directly changes the observed depth, as the depth is indeed greater in the direction specified. By combining Snell's law and basic trigonometry we arrive at a correction coefficient of

$$x_\alpha = \sqrt{1 - \left(\frac{n_1}{n_2} \sin \alpha\right)^2}, \tag{15}$$

where n_1 and n_2 are refractive indices for air and water, respectively. In relation to Figure 6, $D_w = x_\alpha x$, or more importantly $D_w = x_\alpha l_w$: This formula allows us to compute the difference between the length of the beam path in water l_w and the vertical depth of the water layer D_w.

As discussed earlier, there are small differences in the refractive spectra of the SW-IR-wavelengths used in our measurement. They would thus have slightly dif-

ferent refractive indices, adding a small spectral element to this effect. This effect is however once again shadowed by the absorption differences.

The reflective effects follow the Fresnel equations discussed earlier. There are two reflections quantifiably affected by measurement angle: air-to-water-surface reflection and the water-to-air-surface reflection. The refractive spectrum of water induces a small spectral error effect, but the effect affects average intensity the most. The angle-dependent Fresnel equation for reflection in 1-to-2 surface for s-polarised light is often stated as

$$R_{12} = \left| \frac{n_1 \cos\theta - n_2 \sqrt{1 - \left(\frac{n_1}{n_2} \sin\theta\right)^2}}{n_1 \cos\theta + n_2 \sqrt{1 - \left(\frac{n_1}{n_2} \sin\theta\right)^2}} \right|^2 . \tag{16}$$

Since light reflected is in essence lost to our sensor, we can assume the two reflections are independent of one another. Assuming the light travels along the same path both ways delightfully bars the possibility of total internal reflection, as any refracted beam of light will travel at an angle more incident than that of the total internal reflection. We will also assume the reflection from pavement is roughly constant. Due to the peculiar symmetry of the situation, the two-phase reflective process simplifies to

$$I_R(\theta) = I_0(1 - R_{12}(\theta))(1 - R_{21}(\theta)) = I_0(1 - R_{12}(\theta))^2. \tag{17}$$

While there is no one correct measurement angle, the MORSE is always installed in a 30°angle for simplicity. In addition to deepening our understanding on the general subject, these equations can be used for corrections to equate the measurements of different measurement angles, and to ascertain sensitivity to the measurement angle.

2.2.5 Pavement quality variation

In mobile measurement the pavement surface observed is constantly changing. This poses a fundamental challenge to spectroscopic measurement: how to determine the absorption spectrum without reference values for no layer? The dry intensity I_0, previously constant, becomes an unknown variable. Since different pavement surfaces have different spectral properties, the change in I_0 is different for each studied intensity I_i. We will note these as I_{0i}. This introduces ample intensity and some spectral error. The difference of colours can be intuited from Figure 7. This adds three unknowns when one recalls Equation (13). Different samples of pavement are of different colour, both inside and outside of the SW-IR-spectrum.

The reason for the fundamentality of the issue is simple: the MORSE sensor is fashioned after the Vaisala DSC-111, a sensor designed for stationary layer thickness measurement [19]. The sensor was never expected to be able to measure reliably on constantly changing surfaces.

However, even stationary measurement struggles with different pavement surface structures. Differences in pavement colour can be easily accounted for in the

stationary measurement, but structural differences in the pavement surface texture can not. The problem of surface structure is embedded in the definitions of depth, which is more closely discussed in Section 2.3.

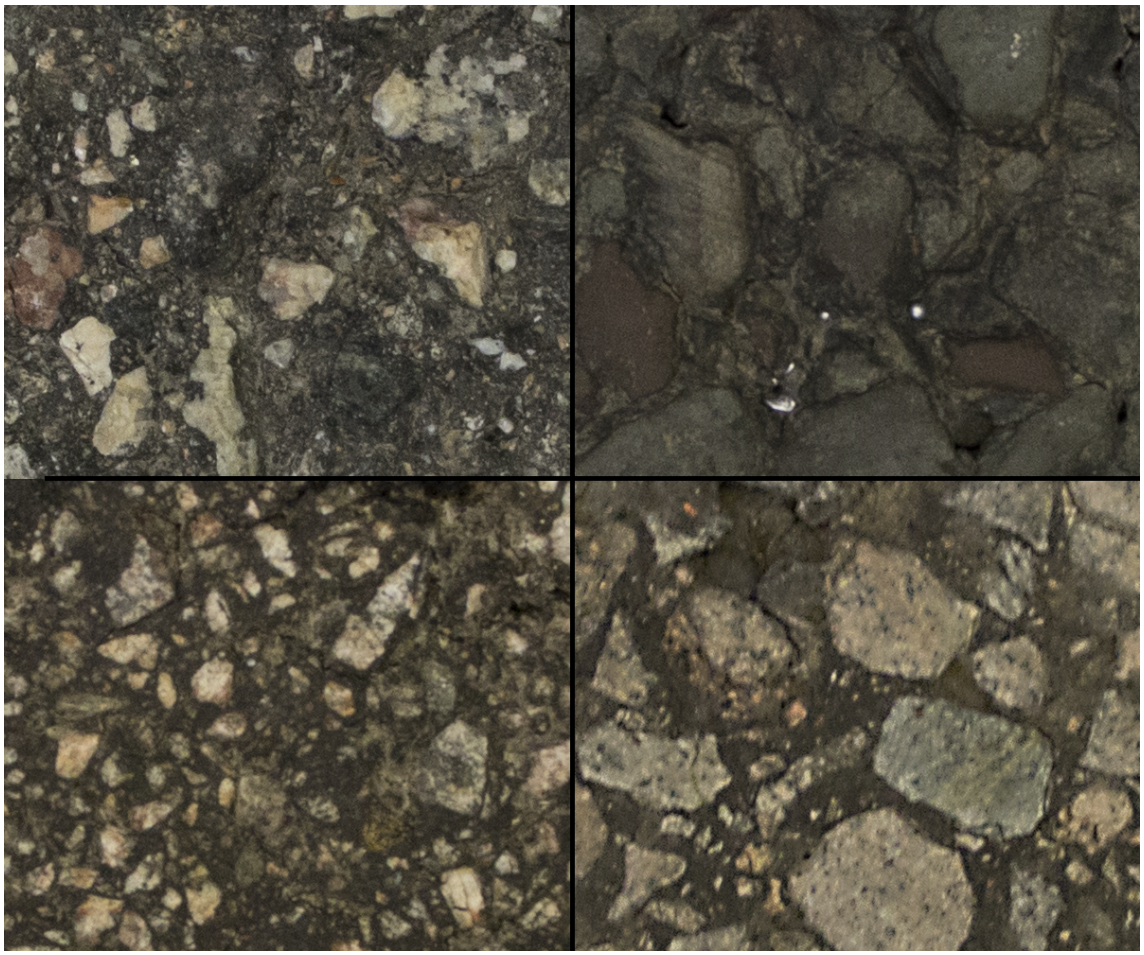

Figure 7: Images of close-up pavement surface with same white balance and to relative scale. The size and colouring of asperities varies from sample to sample.

Peculiarly this is a problem that may be solvable in the mobile measurement, whereas it is not with the stationary sensor. The shorter measurement distance used facilitates rough estimation of relative measurement distance, which could lead to approximation of surface structure. This possibility is discussed in Section 4.6.

Together with the colour variation the structural variation poses a daunting challenge. The previously simple group of Equation (13) is complicated with the changing coloration I_{0i} and unknown pavement height at each lateral location $\overrightarrow{x}$, i.e. $h_p(\overrightarrow{x})$, creating an unknown height distribution. Finding reliable ways to approximate layer thicknesses from this under-defined group of equations is the meat of this thesis.

2.3 Defining depth

Surface of the asphalt pavement has a tricky, fractal-like structure [14]. The concept of depth on such a surface is ambiguous, and sadly many of the studies on this field forgo explicit definition of layer thickness [1]. In practice each measurement method for water amount is another definition for layer thickness, as different methods capture different aspects of the phenomenon, and conversion between them is hard if possible at all. All referenced definitions are illustrated in Figure 9.

Let $\overrightarrow{x}$ be the lateral location on the pavement surface. Then the two key quantities in our definitions are the vertical location (height) of the pavement $h_p(\overrightarrow{x})$ and the vertical location of the water-to-air surface $h_w(\overrightarrow{x})$. These quantities are illustrated in Figure 8. It is notable that these qualities only exist in relation to one another: their absolute values are uninteresting and ill-defined, whereas their difference is the local water depth. Occasionally for simplicity we will treat $h_w(\overrightarrow{x})$ as a constant, representing a level water surface.

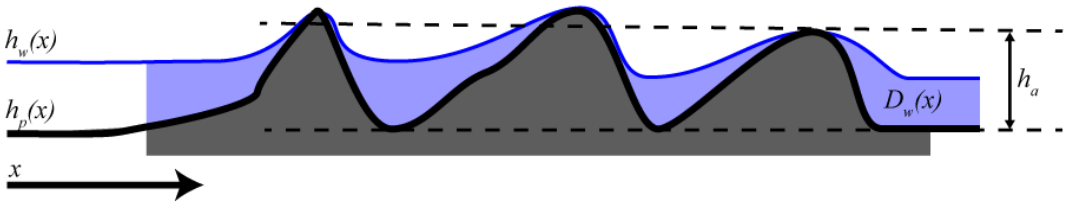

Figure 8: Example of $h_w(\overrightarrow{x})$, $h_p(\overrightarrow{x})$ the vertical locations of the surfaces of water and pavement respectively, their difference, the local depth of water $D_w(x)$ and the average asperity height h_a, which notably is not a function of x. The illustration uses one-dimensional x for clarity.

In 1983, Veith introduced two definitions for different interpretations of water depth relation to surface texture: "above asperity" and centre-line-mean depths. They are perhaps the most widely used formal definitions for water layer thickness [20].

Above asperity depth $D_w(aa)$ was originally defined as the difference between the water surface and "local average asperity height". Average asperity height was defined using a non-standard measurement device, used by Veith in his study. $D_w(aa)$ was the original notation used by Veith, with which we will comply. The notation also holds perhaps unintended wisdom: the water depth is not a function of the pavement or the water amount, but a function of the measurement technique.

The exact measures and functioning of the device were not described in the works cited, or other available sources. We can still conclude the rough method used. The device is described as having densely packed circular measurement sticks, perhaps similar to that of a depth micrometer. These sticks were arranged into a circle. Each stick was lowered until contact with the pavement surface and the average location of these measurement sticks relative to the water surface was used as the depth measurement.

Simplifying this a bit, assuming a square measurement area with side length L

and uniform square measurement sticks with side length G, the above asperity depth is defined as

$$D_w(aa) = h_w - \frac{\sum_{i=1}^{N}\sum_{i=j}^{N} max(h_p(\overrightarrow{x})|\,\overrightarrow{x} \in G_{ij})}{N}, \tag{18}$$

where $\overrightarrow{x}$ is the lateral location, h_w is the vertical location of the water surface (assumed uniform over $\overrightarrow{x}$), and $h_p(\overrightarrow{x})$ is the vertical location of the pavement surface. $N = \lfloor \frac{L}{G} \rfloor$ is the count of squares on each side of the grid. G_{ij} is the ith and jth square of the measurement area divided into a grid, or

$$G_{ij} := \overrightarrow{x}|x_1 \in [(i-1)G, jG] \wedge x_2 \in [(j-1)G, jG]. \tag{19}$$

Centre-line-mean depth $D_w(cla)$, loosely described as total water depth, is generally defined through the volume of the water covering a given area [20]. The water is extracted from a controlled surface area using an absorbent medium with a known weight, then weighed to arrive at an approximation of the mass of the water, from which the volume and then depth are approximated. We use this method to define the total water amount on a test plate using a precision weight scale, thus defining the centre-line-mean depth as follows:

$$D_w(cla) = \frac{m_w/\rho_w}{\hat{A}} \tag{20}$$

Where m_w is the measured total mass of water, ρ is the density of water, and $\hat{A}$ is the area of the test plate. The centre-line-average has been somewhat universally accepted as the ubiquitous definition of average water depth on road surfaces, likely due to its apparent unambiguity. An alternative definition in the same terms as $D_w(aa)$ uses would be

$$D_w(cla) = \frac{\int\int_{\hat{A}} h_w(\overrightarrow{x}) - h_p(\overrightarrow{x}) d\overrightarrow{x}}{\hat{A}}, \tag{21}$$

where A is the measurement area and $||A|| = \hat{A}$. This definition will be referred to later, as it is useful for the closed form analysis of the optical properties of the surface though the measurement method used varies.

A third, practically motivated definition was used by Cerezo et al [1]. Their initial equivalent depth, $D_w(ie)$ was defined similarly to Veith's $D_w(cla)$, but rather than extracting the water via an absorbent cloth they measured the volume applied on a controlled surface area. It should be obvious $D_w(cla) < D_w(ie)$, as the water contained in cracks and the general microtexture of the pavement is not absorbed in the extraction process: an asphalt surface will remain moist even after being dried with a towel.

Finally, we note that the MORSE sensor fundamentally measures local effective optical depth, $D_w(eo)$, due to its reliance on light absorption in the medium. The effective optical depth can in theory be calculated from the extinction equations as an exponentially weighed average depth that sits between that of $D_w(aa)$ and

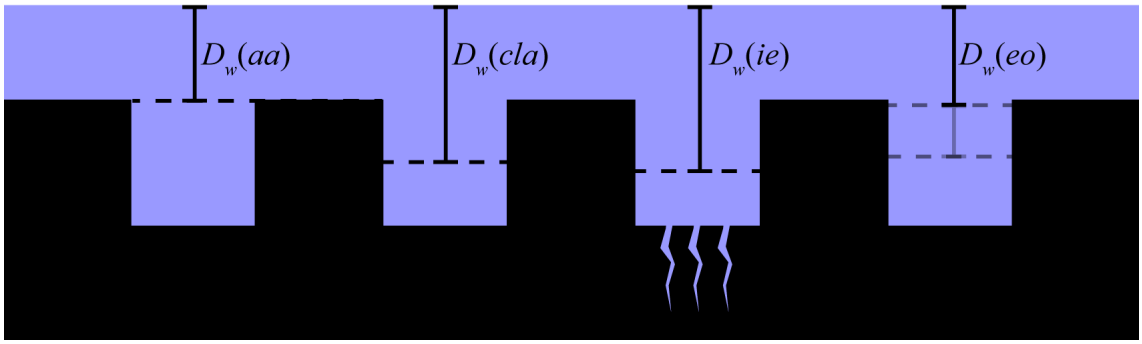

Figure 9: Illustration of the different definitions for water depth on road surface, assuming uniform square wave surface.

$D_w(cla)$. We achieve this through application of Equations (9) and (10), on each individual point $\overrightarrow{x}$ and then their average, respectively.

$$D_w(eo) = -\frac{1}{2\kappa} ln \left(\frac{\int^A e^{-2\kappa(h_w(\overrightarrow{x}) - h_p(\overrightarrow{x}))} d\overrightarrow{x}}{||A||} \right), \tag{22}$$

where κ is the extinction coefficient for water. The extinction process is covered in detail in Section 2.1.2. Areas with lower layer thicknesses dominate the signal due to exponential light absorption, so the average depth is skewed towards the $D_w(aa)$. It should be noted that for non-trivial surface structure the depth is dependent on κ: the effective optical water depth is different for even the three wavelengths used.

Do note that Equation (22) is not used in any of our computation, but is rather presented for comparison and better understanding. Actually using this definition would require good information on the pavement height distribution.

Even assuming the water surface to be flat, i.e. $h_w(\overrightarrow{x})$ a constant, the definitions are related to one another in a complex way. Most importantly, the same $D_w(cla)$ can correspond to multiple different $D_w(eo)$, dependent on the surface geometry (or more specifically, height distribution) $h_p(\overrightarrow{x})$: the measurement results are ambiguous in relation to the other definitions of depth.

When measuring, we know only the effective optical depth $D_w(eo)$, but not h_w or h_p. Without some knowledge of the height distribution of the pavement, we are unable to link our definitions to one another. This is known to cause notable $\pm 50\%$ errors to thickness estimates in extreme cases, those of slick surfaces with little changes in h_p, and those of highly textured surfaces with very high differences in h_p.

The issue of defining depth is ambiguous, and definitions through measurement are the only practical solution: What good is a definition that can't be measured or quantified? In our opinion, the effective optical depth is a valid definition in its own right, but for validation and comparability it should be linked to the other definitions.

2.3.1 Different definitions in action

In his pioneering work in 1980's Veith established a connection between water layers and friction. Veith's aim was to determine sufficient 'worst case conditions' for practical friction testing: how thick a water layer should be considered representative of the worst road conditions e.g. a tire manufacturer should test for. Thus Veith paid little attention to thinner layers, considering thicknesses below 0.3 mm "unreasonable" [20].

Veith posited an exponential connection between friction and layer thickness, previously confirmed by many on his contemporaries, and later by Kulakowski and Hardwood in the 1990's. Their aim was to determine a so called critical water depth, at which, according to their definition, 75% of original friction had been lost. They had specific interest in thin water layers, but were limited in their measurement methods: they used their own version of above asperity depth $D_w(aa)$. As Veith already pointed out, $D_w(aa)$ is systematically lower than other definitions of water depth. Layers studied by Kulakowski and Hardwood were as thin as 0.05 mm in the $D_w(aa)$ sense, and they too arrived at a exponential function describing the loss of friction due to water layers [6].

In their work "Effect of thin water layer on tire/road friction" V. Cerezo et al. describe the connection between thin water layers and friction. The layers they study are thinner than ones studied in road context previously by Veith or Kulakowski and Hardwood. By introducing a third definition for water layer thickness, Initial equivalent depth $D_w(ie)$, they capture behaviour novel previously unrecognised though hinted to by Veith: very thin water layers have no effect on the friction. Previous studies concentrated mostly on thicker layers of water, ignoring the behaviour at low thicknesses. They recognise three distinct phases of road-tire-lubrication, in accordance with tribology, the study of friction and lubrication: Dry contact, boundary lubrication, mixed lubrication and full hydrodynamic lubrication, corresponding to dry fiction, viscoplaning and hydroplaning in the road context [1].

By combining the three works discussed one can conclude that the difference in reported friction behaviour is caused by the careless use of thickness definitions. If we compare the three results and account for the differences between the three definitions for layer thickness, the measurements and models of the three studies across decades conform quite well. The differences between each definition were confirmed by laboratory measurements for different surfaces.

2.4 Asperities

Asphalt concrete is a mixture of bituminous binder and mineral aggregate, i.e. crushed stone particles, often mixed in size. The binder surface wears in use, revealing the more resilient aggregate surface. A popular simplification is to consider the binder agent flat surface containing coarse aggregate particles. The distribution, shape, and size of the particles define the macrotexture of the road surface, while their finer structure defines the microtexture.

This simplification can make the previously complex $h_w(\overrightarrow{x})$ more manageable.

By assuming the pavement to consist of a flat surface with evenly sized asperities, $h_w(\overrightarrow{x})$ can be supplanted with h_a, the (average) asperity height. This simplifies the computation of the height distribution considerably, and is used in later sections.

In Figures 10 and 11 one can observe examples of road surface macro-texture. The piece in Figure 11 shows large aggregate pieces encased in the bituminous binder. The piece is from between the lanes on the Finnish national road 50. These stones will later reveal themselves once the smaller surface stones have been dislocated. One can also observe the rough self-similarity of the pavement surface. This fractal nature of pavement surfaces can be useful for approximating the profile of pavement surfaces [14].

Figure 10: Asphalt surface profile closeup, imaged via photogrammetry, scaled 1:10

Figure 11: Picture of old road pavement cross-section from Finnish national road 50, to scale. Note the differing aggregate size and the bitumen binder. This is not the same piece of pavement as in Figure 10. Top of the picture is the road surface.

Pavement profiles are traditionally roughly categorised by two features: roughness and harshness. Rough surfaces have high macrostructure variation, defined generally as changes with wavelength of 0.5 mm and up. Surfaces with low roughness are called smooth. Correspondingly harsh surfaces vary greatly below the wavelength of 0.5 mm and are opposite to polished surfaces [11]. This terminology goes back to 1980's and accurately captures both the dependency of speed and water layer effects on friction [20]. Harshness or high micro-structure is the main factor determining friction, while roughness mitigates the friction loss caused by both high speeds and water layers. These definitions are illustrated in Figure 12.

Roughness information should be sufficient for determining the relation between effective optical depth $D_w(eo)$ and other definitions, as the micro-structure generally

features lower height changes, limiting the voluminous definition error. However information on the micro-structure would be valuable due to its pivotal role in friction approximation.

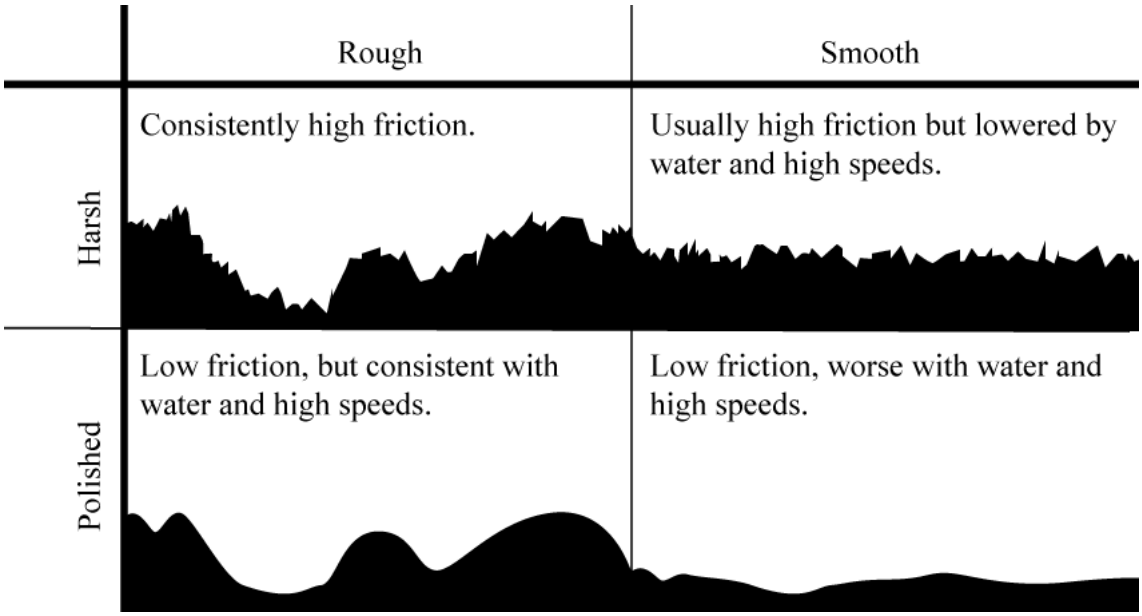

Figure 12: Different types of pavement according to the roughness-harshness-dichotomy.

3 Materials and methods

Reliable reference measurements are required for determining the performance of a thickness model. This further requires a method for accurately manipulating and measuring water and ice layer thicknesses, which are then measured by the studied sensor. These reference measurements form the backbone of this research. In this section we go over the methods used for accurate manipulation and measurement of the reference layer thicknesses.

Most of the reference measurement setup is visible in Figure 13: the setup is rather simple, but surprisingly effective. The pavement samples are used as simulations of road surface, and the micrometer and the precision weight scale are used to determine the thickness of the water layer on them. The freezing plate occupies the background of the picture and it is used for freezing the water for ice layer measurement.

Figure 13: Key pieces of the test setup: pavement samples, precision scale, depth micrometer, all on the custom freezer plate. MORSE not in the picture.

3.1 Pavement samples

Previous research has struggled with procuring representative pavement samples for laboratory measurements. For an example in [1] Cerezo used samples constructed from small stones in a laboratory, lacking in the usual wear of pavement and bitumen. Alternative solutions include a specialized "pavement wear machine" called the Wehner/Schulze (W/S) machine that simulates the effect of traffic [18]. Cutting samples from actual road surface in use is preferable, but necessitates special equipment and the stopping of traffic, in addition to creating the problem of the hole in the road. Most of the samples in our study were collected from roads being due for new pavement: before a new asphalt surface is laid, the old surface is milled to

roughen it up, creating a stronger bond between the layers. Combining the collection of the samples with the pavement laying work-sites solves most of the problems of collection, but limits the collection to rather old and worn pavements.

The thick pieces of pavement are next horizontally cut into thinner slices. This both makes the pieces easier to handle and increases heat transfer through the piece, which is integral for the measurement of ice. Due to the choice of the freezer plate in this study, the heat conductivity of the samples was essential to allow any freezing to take place. The choice of the freezer plate over a climactic chamber was motivated by cost and convenience. To ensure heat conductivity, a layer of lead is moulted on to the bottom of the piece. This both increases the contact surface with the freezer plate and water-proofs the bottom of the piece, though the process itself is quite laborious. The test pieces used in this study are visible in Figure 15. One can also see the progression in test piece design progressing in the same Figure.

Aside from the bottom the test piece is moulded with two-component plastic sealant on all sides. Once hardened, the plastic is both lightweight, durable and rigid, which is important since both the thin layer of pavement and the leaden bottom are flexible and fragile. The moulded plastic provides some much needed structural integrity to the piece. The piece is finished with poly-urethane walls to keep water from flowing away. The structure is visible in Figure 14. The test pieces constructed in this way are representative and easy to handle, being lightweight and durable.

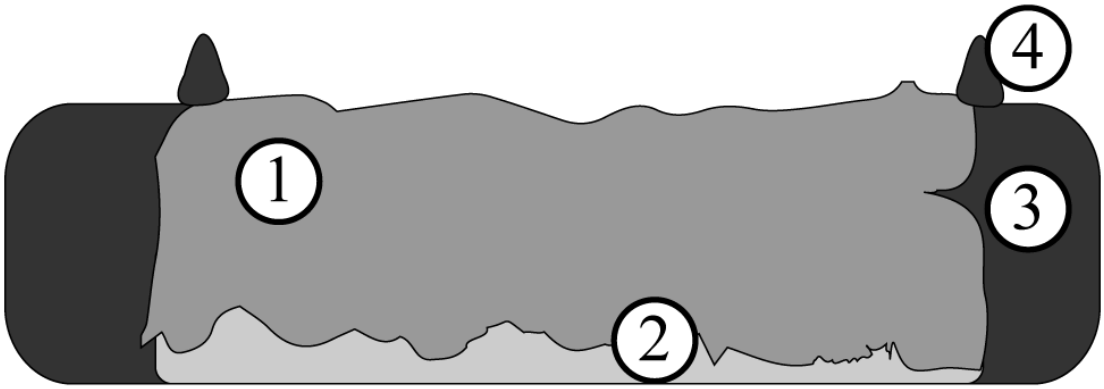

Figure 14: Structure of a finished pavement sample

1. Thin-cut piece of pavement
2. Leaden, water-proof, heat-conducting bottom
3. Moulded plastic walls to ensure structural integrity
4. Pool walls to prevent water from escaping

We also use roofing felt as an alternative material for test pieces. The roofing felt surface is roughly similar to asphalt concrete in surface structure, as both feature stone aggregate bound together with bitumen though they differ largely in particle

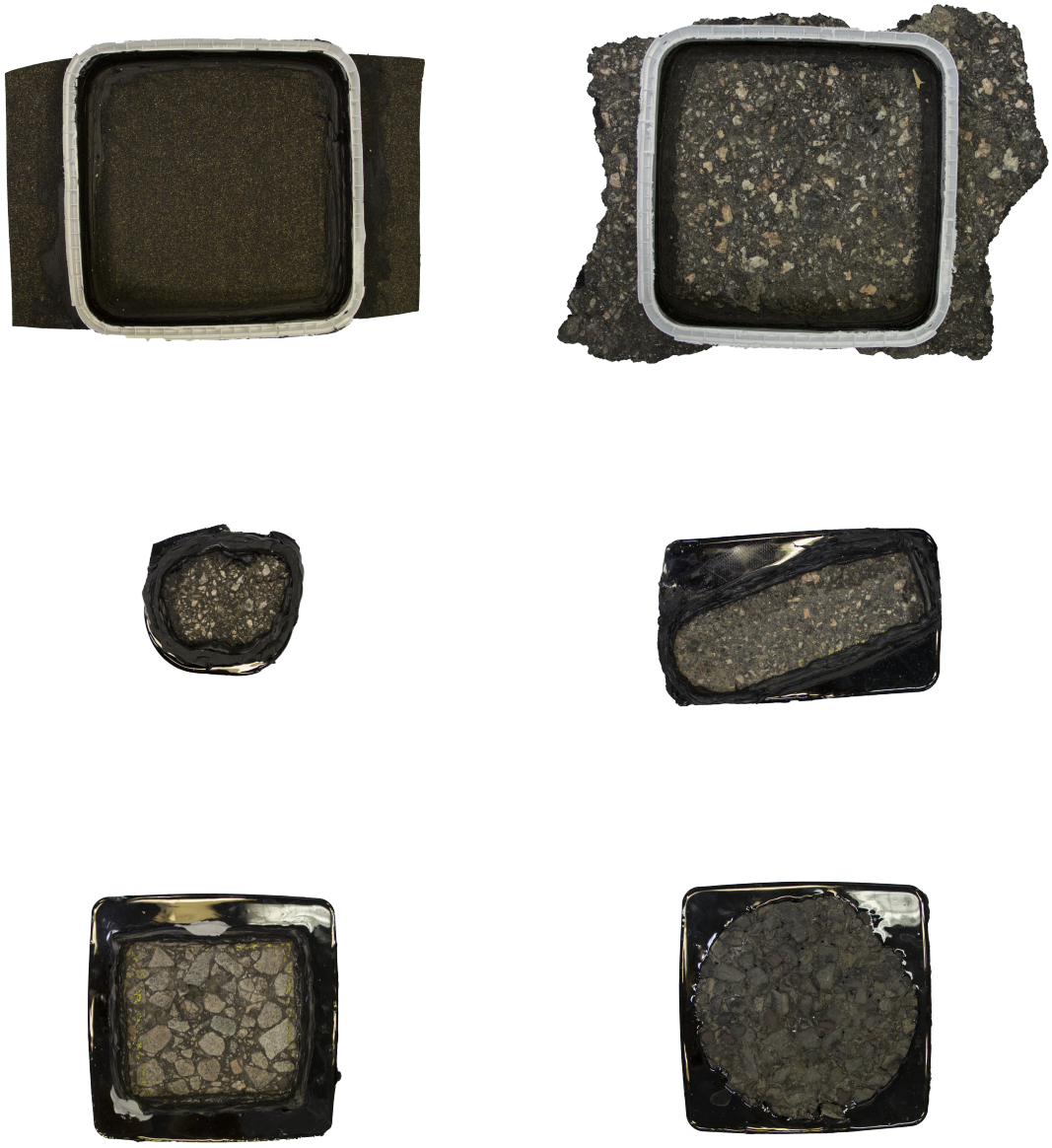

Figure 15: Test pieces used in this study, to relative scale. The evolution of the test piece concept progresses from up to down.

size and internal structure. Thus we can only consider roofing felt an approximation of an actual road surface. It provides fewer technical challenges, so it is deemed valuable in use nonetheless. Unlike asphalt concrete roofing felt is lightweight, readily water-proof, flat and smoother, thinner and operable with regular scissors.

3.2 Controlling and measuring water layers

Of the phenomena covered, water layers on the road surface, are the most prevalent and easiest to study. Rough manipulation of water layer thickness is possible with just a syringe, adding and removing water as needed. More exact manipulation calls for equally more exact methods. We aim for a precision of 10 µm matching the resolution of the DSC-111 Remote Road Sensor [19], in the range from 0 to 10 mm.

Instead of manually manipulating the layer thickness by adding and removing water, we allow the water to evaporate, thus passively manipulating the layer thickness. This way we can scan all layer thicknesses thinner than the starting thickness.

Passive manipulation translates the original problem of controlling layer thicknesses to measuring them. To this end, we employ two measurement tools: depth micrometer and precision scale.

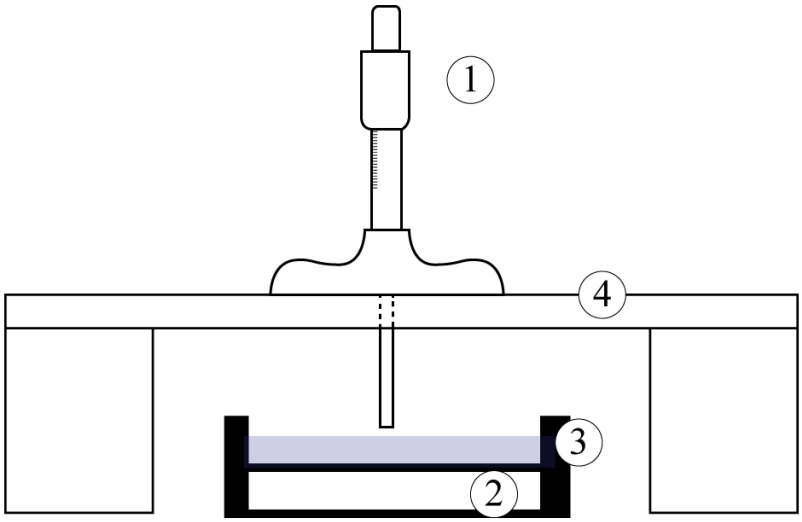

Figure 16: Elements of test setup:

1. Depth micrometer
2. Measurement plate
3. Water-resistant boundary
4. Stable rack

The depth micrometer is used to measure the location of the water surface relative to a stable measurement rack, see Figure 16. The tip of the depth micrometer is then lowered until it makes visible contact with the water surface: the contact is evident from the following surface tension reaction, presented in Figure 17. This offers us a reproducible measurement of the surface location, or $\Delta D_w(aa)$, as per Section 2.3. By fitting a linear equation to the micrometer measurement points we eliminate random micrometer measurement error and arrive at a very precise estimate of the relative water surface location.

Figure 17: The visual effect of the surface tension used to identify contact with water surface.

The micrometer measurement method is however prone to bias-type error when determining the layer thickness: it is unclear when exactly the surface tension occurs. Once the linear fitting has removed any noise, we are still left with any bias present. When the water surface is on average below the asperity height, it can no longer be accurately traced with the micrometer.

The average water depth, effectively $D_w(ie)$ in this case, is measured using a high precision weight scale. The scale provides more frequent measurement than the micrometer and does not disturb the sensor. The precision scale can also accurately measure very thin layers, assuming the surface is generally even. It is however less flexible in its use, and strongly affected by general unevenness of the surface studied.

Surprisingly no prior road surface water layer related research using evaporation as a thickness manipulation method was found, while micrometer and precision scale have been used from the very beginning of road surface layer measurements.

3.2.1 Linearity of water evaporation

We use a fan to accelerate the evaporation. The air flow velocity of 4 meters per second we can produce with a consumer grade table fan increases the evaporation rate approximately ten-fold compared to ambient air flow, both according to prior research and our experiments.[4] This increase in evaporation rate out-weights any caused by changes in ambient air flow caused by changes in the air conditioning and general level of human activity around the measurement area.

The benefits of the accelerated evaporation are two-fold: assuming air temperature and humidity stay roughly constant throughout the measurement, the evaporation rate is also constant in our setup. This has been confirmed with both micrometer and precision scale measurements. Accelerated evaporation also makes the measurement considerably faster, both saving time on experimentation and further lessening the effect of other environmental factors, such as the temperature and humidity drift throughout the day.

According to our measurements, the water evaporation rate is very linear until the end of the process: once the asphalt surface is revealed from under the water, added evaporation surface area and other factors may change the evaporation rate. The assumption of linear evaporation still holds for most of the measurement and is a useful tool for averaging and interpolating reference values.

3.3 Controlling ice

Ice layer manipulation is executed similarly to that of water layers. The measurement plate is cooled down with a custom-made refrigeration unit, then covered with water.

The water is allowed to freeze into ice and then melted with a heat blower. Once the ice is completely melted the remaining water is allowed to refreeze. By adjusting the heat and fan power, water can be either evaporated off or condensated onto the measurement plate, allowing for both increasing and decreasing ice levels. The fan and heater are controlled with a time switch, which turns the power on and off at suitable intervals.

An important benefit of the melting cycle is the clarity of the ice: if left to room temperature air, water will condensate onto the ice surface, forming white, opaque frost. In our method the ice is very clear once formed, and once again when the heater starts and melts the frost momentarily. This both allows us to reproduce similar ice surfaces of different thickness, and to compare the responses of different types of ice surfaces to known water thicknesses, if the ice layer is fully melted during the melting phase.

Unlike the water measurement, this cyclical melting and refreezing of ice does not produce continuous results, but it functions quite well as a passive measurement, requiring no user input: the sensor and the fans can be left to themselves, producing several thicknesses over the span of hours.

By measuring the water layer thickness when water is liquid, one can achieve results identical to those for water, accounting for expansion during freezing. The test can also function as its own reference: by measuring the amount of water once liquid we arrive at a reasonably reliable reference: the amount of the water should not depend on the phase, barring expansion on freezing. This is useful due to the poor performance of both the precision scale and the micrometer for ice. The scale can't differentiate between frost and dew condensed from the air onto the sample walls and the actual ice surface measured, and thus generally performs poorly with ice samples. The micrometer tends to melt the ice. This both makes confirmation of contact ambiguous and disturbs the surface measured.

For our references in this study we will be using the sameness requirement, as it is trivial to implement and is ultimately quite a strict requirement for the measurements.

3.3.1 Water measurement as absolute reference for ice measurement

As an alternative to measuring the water layer thickness between freezing events or simply measuring the sameness of the water surface, the water measurement may be conducted prior to ice measurement, and then used as the reference for correct amount of ice.

For most testing it suffices to require the sameness of water and ice amounts: should the sensor measure correctly, the two quantities should be the same. When an absolute reference is required, it can be derived from the water measurement as well though backwards computation from the water performance, i.e. correcting the water measurement with an ad hoc -function for the measurement setup in question. The errors in water measurement are reliably systematic, should the test setup, location and distance of the sample, remain constant. With the ad hoc -function the equivalents for absolute thicknesses measured with the reliable reference measurements can be derived from the sensor's own water measurement.

This method is useful when absolute information on the ice performance is required.

3.4 Measurement cycle

We will go over the measurement cycle roughly to explain the capabilities and limitations created by the spatio-temporal resolution. One complete measurement cycle lasts roughly 25 ms. Assuming the measurement device is moving at the speed of 60 km/h, one such cycle would thus average the length of approximately 40 cm. The laser signals are modulated at a rate of 1 kHz to 2 kHz. The sample rate of the integrating intensity meter is 10 kHz, corresponding to an averaged length of 0.15 cm. Lastly the diameter of the area illuminated by each of the measurement lasers is 2.5 cm. All of these quantities naturally depend on the measurement distance.

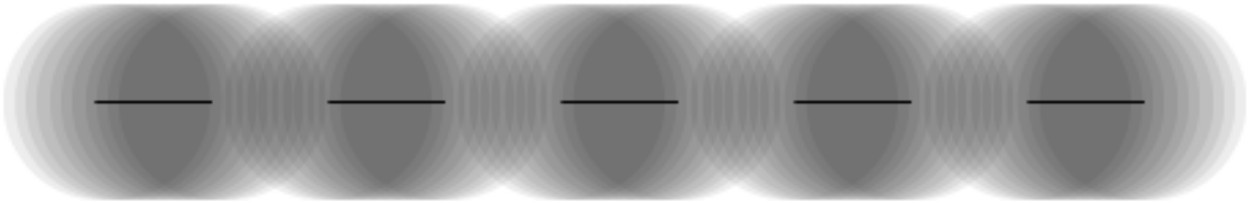

Figure 18: Trace of partial measurement cycle for a single laser, to scale assuming speed of 60 km h^{-1}. Each individual area averaged by the integrating intensity meter and illuminated by the laser cone is marked with a partially transparent circle. The dark dashed line is the path of the centre of the cone of the laser.

The trace of this measurement cycle is presented in Figure 18. It demonstrates above all the scope of deconvolution required to discern between smaller features of the pavement: while the spatio-temporal resolution of the integrating intensity meter is in theory sufficient for macro-structure analysis, the large overlap of the laser cones causes the relative change between samples to be quite small.

4 Modelling

In modelling we arrive at a threefold problem. Firstly we must define a reliable thickness reference for the measurements. Since thickness is somewhat ill-defined by nature this is not a trivial task. Secondly, we must define performance: what would we expect of a good model? Thirdly and lastly, we test our models against the given references and performance metrics, while trying to guarantee that the models can be generalised: they should not only perform well on our ultimately limited laboratory measurements, but in a wide variety of measurement situations.

4.1 Deriving reliable reference from measurements

We have three main ways of measuring water layer thickness: The MORSE sensor itself, depth micrometer measurements and precision scale. All of these are limited and flawed in their own ways. Combining these three methods into one reliable reference thickness is the first task in analysing and improving our algorithms.

The micrometer measurement is arduous and only measures the location of the water surface: once the surface is no longer even, i.e. the highest asperities of the pavement pierce the surface, the measurement becomes rather unreliable, as the location of the measurement changes the result. In other words, the micrometre can't measure very thin layers. In addition, the location information is not absolute but relative to the stationary stable rack, as the height of the "bottom", and thus water depth, depends on the exact measurement location. The micrometer is however the only direct measurement of water amount: one millimetre change in surface location is definitely a one millimetre change in layer thickness.

The precision scale provides continuous measurement with little user intervention required. It thus captures well any non-linear drying behaviour. It is however an indirect measurement of the water thickness: the conversion factor between grams and millimetres has to be defined for each test piece. Furthermore, once the surface is almost dry, leftover water is often packed in the crevices and corners of the test piece. In this situation, the definitions on water depth disagree, as the scale can still report some residue water, while all other definitions agree on dry.

Finally, the MORSE can hardly be used as a reference for its own water measurement, for obvious reasons of circularity. It is however very reliable at deducing when the surface is dry: when the optical signals of the pavement match those of dry pavement, the surface is unarguably dry. Due to the darkening effect mentioned in Section 2.2.3 this is also easily confirmed with visually, as the difference in tone between a moist and a dry surface is stark.

As a shrewd reader could deduce from this introduction, the three measurements complement one another, mitigating the shortcomings of one another. The direct measurement with the micrometer can be used to provide the conversion factor from grams to millimetres for the precision scale, the scale produces a continuous water measurement and the MORSE can be used to define when the surface is dried. In other words, the micrometer results are used to scale the scale results, and then the MORSE results set the correct x-intercept. The scale provides the continuity of

measurement data and captures any potential non-linearities.

4.2 Reference definition

For the purposes of this work, the laboratory measurements are treated as the correct results, and the models are judged on their ability to recreate the layer thicknesses. This may lead to impossible requirements for the model: the exact same signal values may be attained with different combinations of layer thicknesses. This sets an upper bound for model performance.

4.2.1 Lenient specification trapezoidal error

For defining goodness of fit, a measure for the agreement of model results and reference layers is required. This measure tells us how far off the model is from the truth.

For an example, the mean square error (MSE) is a traditional choice for measuring error. In MSE the overall error is the mean of the squared errors between the estimated values (e.g. reference water layer thickness) and the estimations (the results of a thickness model). Thus this error function disproportionately punishes large errors. Considering an estimator $\hat{Y}$ for the reference values Y, we would define the mean squared error as

$$MSE(\hat{Y}) = \frac{1}{n}\sum_{i=1}^{n}(Y_i - \hat{Y}_i)^2. \tag{23}$$

This equation is however only included for comparison. Using the absolute mean square error would produce rather strange results, so we will set our own requirements for the error function used.

We wish to add leniency corresponding to the accuracy specification of the sensor: absolute 0.1 mm under the depth of 1 mm, and 10% relative error above [19]. For simplicity we will use absolute tolerance of 0.05 mm and relative tolerance of 5% everywhere rather than the piece-wise defined error discussed. The reasoning for this is two-fold: it is better to contain all results within the accuracy specification than to have some of them very close to the reference. Since the accuracy specification for the application is quite lenient this actually plays a significant role. This also allows for some potential measurement error in the reference measurements.

Secondly, we study relative error, similarly due to application needs: more accurate measurements are required in the lower thicknesses. Lastly, we measure trapezoidal average error due to the differing density of the measurement data. Due to the evaporation measurement method, Y_i is monotonous in relation to i for each measurement series. Thus we can safely construct trapezoids of the values $\hat{Y}_i$. The area of the combination of the trapezoids is neutral to measurement point density, i.e. denser series are not weighed more as in MSE.

The error function we use is defined thus as

$$E(\hat{Y}) = \sum_{i=2}^{n} max \left\{ 0, \left(\frac{max\left\{ \left| Y_i - \hat{Y}_i \right| - 0.05, 0 \right\}}{Y_i + 0.01} + \frac{max\left\{ \left| Y_{i-1} - \hat{Y}_{i-1} \right| - 0.05, 0 \right\}}{Y_{i-1} + 0.01} \right) \frac{|Y_i - Y_{i-1}|}{2} - 0.05 \right\}. \tag{24}$$

Here $\hat{Y}$ could be, for an example, the water layer thickness reported by the model, while Y would then be the reference thickness. The same equation is used for determining error in ice layer thickness, and the final result is the sum of the two.

4.3 Baseline algorithm

The prototype model at the time of writing is a polynomial fraction equation, internally called "generalised ratio formula". In essence, the three raw signals that are given as input are scaled such that the signal value for each laser when the surface is dry is 1, and all other parameters on the equations are free parameters optimised for the best performance based on a reference data set. The polynomial fraction seemingly both succeeds in capturing some of the spectral behaviour and being malleable enough to be optimised.

In mobile road detection this model can suffer from inaccurate dry scaling, since the absolute signal values are affected by the changing road surface: a patch of road may induce higher or lower signal values depending on the colour and texture of the patch. As discussed, this poses somewhat of a fundamental problem to thickness models, as it is easiest to assume that the dry reflectivity would stay constant.

The model is very frugal both in terms of memory and computation, as it only requires storing and evaluating the single polynomial. It is thus an effective baseline for other algorithms: any trade-offs in memory or performance should be offset by gained performance.

4.4 Physical model

A simple physically inspired model can be constructed from the uniform Lambert law of absorbency and the physical complications mentioned in section 2.1.2 with a couple of assumptions, specifically prior knowledge of the dry responses I_0 of potential road surfaces. The gist of the model is to compute the most likely dry road surface covered by the studied layer while simultaneously computing the most likely layer thickness. Using the simplest version of the physical situation we can start with

$$I_i = I_{01} e^{-2l\kappa_i}, \tag{25}$$

where the indices i denote the index of the wavelength used. We will add a uniform scaling factor D for the darkening effect described in Section 2.2.3 and

rearrange the equation to

$$I_{0i}e^{-2l\kappa_i}D - I_i = 0. \tag{26}$$

Now, assuming we have N different known dry values I_{0_n}, we can compute the most likely dry value - layer thickness pair by finding the minimum of the left hand side of the equation. This naturally assumes the physical behaviour used to be exact enough to simulate the layer thicknesses reliably, the surface studied to be indeed one of, or spectrally close to one of the N known dry values, and the closest point to be the most likely one. Using simple euclidean distance to measure the distance we would arrive at

$$min_{n,l}\left(\sum_{i=1}^{3}\left(I_{0i_n}e^{-2l\kappa_i}D - I_i\right)^2\right). \tag{27}$$

By finding the layer thickness and dry reference that minimise the error between the simulated signal levels and the measured levels we arrive at an estimation of the layer thickness. By including information on surface temperature, reasonable layer thickness approximations with mixed water and ice layers are possible.

The main strength of this model is our ability to improve it as our understanding of the measurement situation improves, and vice versa: it encourages efforts to further our understanding. For an example, adding a layer thickness dependence to the parameter D allows to approximate very thin layers more accurately, if we study the effect enough to reliably model it. In other words, for such a straight-forward model the process of improvement is clear and intuitive, and encourages deepening the fundamental understanding of the measurement situation.

The model could also be used simply to pick the dry reference for any other algorithm that assumes the I_0 to be known.

We also attempted adding a function for the roughness of the road, that in essence eliminates the effect of the definition difference presented in Equation (22). The roughness is also tied to the road type: allowing for the roughness to be used as an optimisation parameter would allow for over-optimisation. This brings us to a roughness function as $\rho(l, n)$, where l is the layer thickness and n the road type. Then the algorithm would minimise the target function, that is

$$min_{n,l}\left(\sum_{i=1}^{3}\left(I_{0i_n}e^{-2l\kappa_i\rho(l,n)}D(l) - I_i\right)^2\right) \tag{28}$$

By choosing easily differentiable functions for ρ and D the computational complexity of the problem could be reduced.

The main weakness of the model is reliance on the pre-existing dry reference information: a mismatch of references severely hampers the performance of the model. Furthermore the relevant reference values depend on the area the sensor is used in. The same problem holds for the roughness parameter tied to the road type: the roughness parameter has to be specified for each road type. Since roads in

different areas differ, creating and maintaining a complete library of all the relevant road types would be an arduous task.

An interesting solution to this problem outside the scope of this thesis are Self organising maps (SOMs), also called Kohonen maps, introduced in detail in [5]. The SOM is an unsupervised machine learning clustering algorithm: given data points, the SOM clusters them into groups with similar properties. In effect, it could recognise the most common road types for each area, providing the dry reference information for the physical algorithm. The SOM is very frugal computationally and memory-wise, as each data point can be updated separately without the need to store or reteach large data sets. Similar machine learning solutions could be used to estimate the roughness parameter for each road type, eliminating the task of manual road quality study. The use of SOM would require a separate algorithm for assessing whether the observed road is dry.

Another flaw of this approach is the computational expense of the minimisation process. With mixed layers there are two unknown parameters, rendering the process computationally cumbersome. For pure water or ice layers the computation is considerably cheaper, as the derivative can be computed analytically, and the optima then found by searching for the roots of the new equation, a problem for which multiple efficient solutions exist, especially given that we can pick and choose easily differentiable equations for our model.

4.5 Compacted Look-up-table

It is naturally possible to construct a look-up-table (LUT) from the laboratory measurements. Through careful smoothing, interpolation and extrapolation the general trends visible in the data can be generalised, avoiding specificity to our laboratory measurements.

4.5.1 Selecting dimensions

The dimensions chosen define the properties of the look-up-table. For computational efficiency we will use a two-dimensional LUT: This allows much finer tables to be used and leads to better generalisation. For an example we can consider the dimensions $\{\frac{I_1}{I_3}, \frac{I_2}{I_3}\}$. This option is brightness-agnostic: uniform changes to brightness would not cause changes in reported layer thicknesses, following the original intent of the reference wavelength. Since most of the error sources, namely pavement colour variation, are highly uniform, this choice of dimensions allows us to ignore the main source of measurement error.

4.5.2 Interpolation, smoothness and continuity

Since the entirety of the parameter space is not covered by measurements, i.e. we don't have all different combinations of layers, some interpolation is required. Also to ensure sufficient continuity in measurement, the values should be averaged and smoothed.

This is achieved by first binning the parameter space. Then the contents of each bin are averaged. Each bin may contain measurements from several different pavement types with differing water or ice layers.

Next a weight of 1 is issued to all non-empty bins, while the empty bins have zero weight. The weights are then smoothed and interpolated by convoluting the weights with a Gaussian mask. Lastly, a weighed average is computed for each bin using the newly filtered weights. This way the empty bins are filled with the weighed averages of the measurements of the nearby bins, and the already filled bins are smoothed.

4.5.3 Updating and modifying the LUT

Perhaps the most notable upside of the LUT is the ease of updating and modifying it: simply by introducing new values to the data set used to construct it and repeating the assembly process automatically fits this new information together with the old measurements.

Similarly ad hoc values are easy to provide: certain areas in the LUT can be pre-defined as invalid, as certain signal level combinations should not be possible under normal circumstances. Invalidating values could be useful in e.g. recognising unreliable measurements, and prompting the user with an error message.

4.6 In situ roughness analysis

Approximate roughness information would be beneficial in linking the several definitions of water depth together, allowing us to approximate the distribution of $h_p(x)$. This would have to be done in real time to allow water measurement correction.

The general state and feasibility of on-board structural analysis is thoroughly covered in [2]. Most interestingly volumetric roughness definition is shown to be in good general accordance with surface friction.

To this end the surface structure of Finnish national road 11543, Ylästöntie, was charted. The road is roughly 5.2 km long, and features 15 distinct road qualities of different age and wear. The road was chosen for the wide variety of different road qualities in addition to its location less than a kilometre away from the Vaisala office. We assumed uniform wear for each visually uniform stretch of the road: this assumption is most likely slightly flawed, as especially uphill stretches are more worn than flat portions of the road. This assumption was however chosen to allow a lower number of distinct road qualities, as the tactile collection method of the data was rather cumbersome.

Each uniform stretch was analysed in a tactile manner for two qualities: roughness and harshness, as per Figure 12. Both were rated on an index scale from 1 to 5, one being the least rough or harsh, and 5 the most. The analysis was conducted for both the rut worn by the tires and the section of the road directly between the two ruts. The section between the ruts is of the same age and material as the ruts, but much less worn: thus these sections should report much higher roughness and harshness, ceteris paribus. The map of the road section studied together with the surface structure is visible in Figure 19.

The effect of roughness on the reported water amount was then confirmed from historical measurement data on the same road: the tactile surface structure index is in general agreement with MORSE reported liquid layer thickness readings: rougher stretches of road correspond to lower layer thicknesses, just as the theory states. This could be taken to confirm the validity of the tactile analysis of the road surface to an extent.

The road was then studied with the MORSE sensor, by driving along the road recording the raw signal values instead of the processed road weather information. This process was repeated several times for each stretch of the road, both inside and outside of ruts. The location along the road was recorded by video to allow splitting the data according to the different stretches by timestamp.

The raw data was studied with Fourier analysis for high-frequency amplitude peaks, which we theorised would be connected to changes in surface structure.

We also studied overall variance as a more stable measure. We measured the variance of the Fourier amplitude peaks of 256 subsequent sample subsets of the 1024 sample raw signal from the raw signal, i.e. for a sample $\mathbf{S} = (s_i)_{i=1}^{1024}$ we consider the subsets $\mathbf{S}_k = (s_i)_{i=k}^{k+255}$ to arrive at

$$Var^{\star}(\mathbf{S}) = \frac{1}{768\mathcal{F}(S)_{n_1}} \sum_{k=1}^{768} \left(\mathcal{F}(S)_{n_1} - \mathcal{F}(S_k)_{n_2}\right)^2, \tag{29}$$

where $\mathcal{F}(\circ)_n$ is the nth bin of the discrete Fourier transform, and n_2 and n_1 are the corresponding bins in the 256 and 1024 length DFTs respectively. This solution seems to minimize the effect of the other lasers, but still suffers from harmonics of the measurement signals. The star notation is used to discern this definition of relative variance from the standard one.

4.6.1 Friction calculation

Roughness analysis provides another potential application for the sensor: using the surface structure analysis to create an approximation of pavement friction. This would be a valuable addition, as the current sensor can only estimate friction depression due to surface layers. In recent years the possibility of deriving friction estimates from surface structure information has been discussed though the structure information was derived from chromatic white light measurement [18]. However, should the MORSE prove capable of roughness analysis, it could both provide more accurate layer thickness measurements and friction approximations, as surface structure information could be integrated into the calculation of both.

With minor signal fidelity improvements and suitable heuristics we could hope to derive friction approximations on the fly [14].

4.6.2 Square wave analysis

Square wave analysis is a potential method for increasing the fidelity of the raw measurement data. It could prove a valuable tool friction approximation.

The measurement signal consists mainly of the feedback of the three modulated laser signals. Due to the modulation, the signals are roughly square waves with different wavelengths and slightly varying amplitudes. This should not be mistaken for the wavelengths of the lasers. Fourier analysis is used to study the amplitude of the specific modulation wavelengths.

Since the signals studied are square waves, classical Fourier analysis is sub-optimal. It will both underestimate the magnitude of the studied peaks and add Fourier artefacts at the odd multiples of the frequency of the studied peak. In essence, the effect of modulation is spread throughout the spectrum. The problem caused by this is two-fold: the underestimation diminished fidelity, and makes the signal more susceptible to noise. This lowers measurement accuracy and limits the thickness that can be accurately measured. Secondly the artefacts contaminate the higher-frequency noise spectrum, preventing the reliable study of the noise, which contains information on the road surface structure.

Square wave transform (SWT) provides a solution to this problem. The principle of operation is the same as in the Fourier transform, but instead of sinusoidal waves we use square waves as the basis. Square waves do not form a proper orthogonal basis, but for discrete Fourier transform (DFT) the results are equivalent. The mathematical basis of the square wave transform is discussed in depth in [24].

We tested two methods for determining the SWT. The so called "Square wave method" employs a direct approach, representing the fitting of the signal as an N-by-N matrix equation, where N is the number of intervals fitted. As a linear system the N values in the time domain can be transformed into the frequency domain with simple matrix calculus, projecting the values onto the non-orthogonal square basis. For our case, this is the same N =1024 as discussed before [25].

$$\mathbf{M}C = V \tag{30}$$

$$C = \mathbf{M}^{-1}V, \tag{31}$$

where C is a vector containing the SWT-coefficients for different wavelengths and V is the original values at the N intervals. The matrix of coefficients $\mathbf{M}$ is constant, so it can be pre-inverted for efficiency. Then the only expensive operation is the matrix multiplication. MATLAB code for this method is readily provided by the author of [16], so this method is simple to implement. This method however does not consider the phase of the square wave, and is thus limited in actual use. In simulated laboratory measurement environment the three lasers can be phase-locked to eliminate this error completely, so this is a good algorithm for the preliminary testing conducted in this study. The MORSE sensor however does not feature phase-locking, so an alternative computational approach is required. The computational expense of matrix multiplication is quite high, deterring the option to introduce phase-locking to accommodate this solution.

An all-around superior solution does exist for generic non-orthogonal bases, including the square wave. In essence, any periodic function can function as a base, if

one can construct the Fourier series of said function. For example, the square wave can be expressed in terms of the sine wave as

$$sq(\omega) = sin(\omega) + \underbrace{\frac{sin(3\omega)}{3} + \frac{sin(5\omega)}{5} + \frac{sin(7\omega)}{7} + \frac{sin(9\omega)}{9} + \frac{sin(11\omega)}{11} + ...}_{error} \quad (32)$$

As the Fourier series of the square wave states. By subtracting $\frac{sq(3\omega)}{3}$ from both sides we arrive at

$$sq(\omega) - \frac{sq(3\omega)}{3} = sin(\omega) + \underbrace{\frac{sin(5\omega)}{5} + \frac{sin(7\omega)}{7} + \frac{sin(11\omega)}{11} + \frac{sin(13\omega)}{13} + ...}_{error} \quad (33)$$

removing all multiples of three from the equation. If we repeat this for $\frac{sq(5\omega)}{5}$

$$sq(\omega) - \frac{sq(3\omega)}{3} - \frac{sq(5\omega)}{5} = sin(\omega) + \underbrace{\frac{sin(7\omega)}{7} + \frac{sin(11\omega)}{11} + \frac{sin(13\omega)}{13} + ...}_{error} \quad (34)$$

we eliminate once again the largest error term. By continuing this process, we can eliminate the error, as the coefficients become smaller, and the error is pushed to higher frequencies. As the frequency is pushed beyond that of the frequency domain included in the discrete Fourier transform it essentially disappears, as the higher frequencies are ignored. Thus we can accurately approximate the sinusoidal basis with square waves, and by substituting the sine waves with their square-wave approximations arrive at an equivalent square wave decomposition [21].

By applying this process to the sinusoidal base of the Fourier transform we transform the basis into a square one. More generally, this process functions for any basis $S(x)$ with a Fourier transform. This is useful, since the signals are not exactly square waves, due to filtering on the hardware level. Furthermore, the whole process can be computed in the Fourier domain with low computational cost, the total cost being roughly on the scale of two FFT's [22]. As a bonus, the process can be halted without major complications: we can transform just the lower frequencies containing the square waves we wish to study with the technique to further lower the cost.

These techniques allow us to increase the fidelity of our signal, resulting in less noisy measurements. Perhaps even more importantly they clean the noise spectrum, allowing us to better analyse the changes not dependent on the laser modulation.

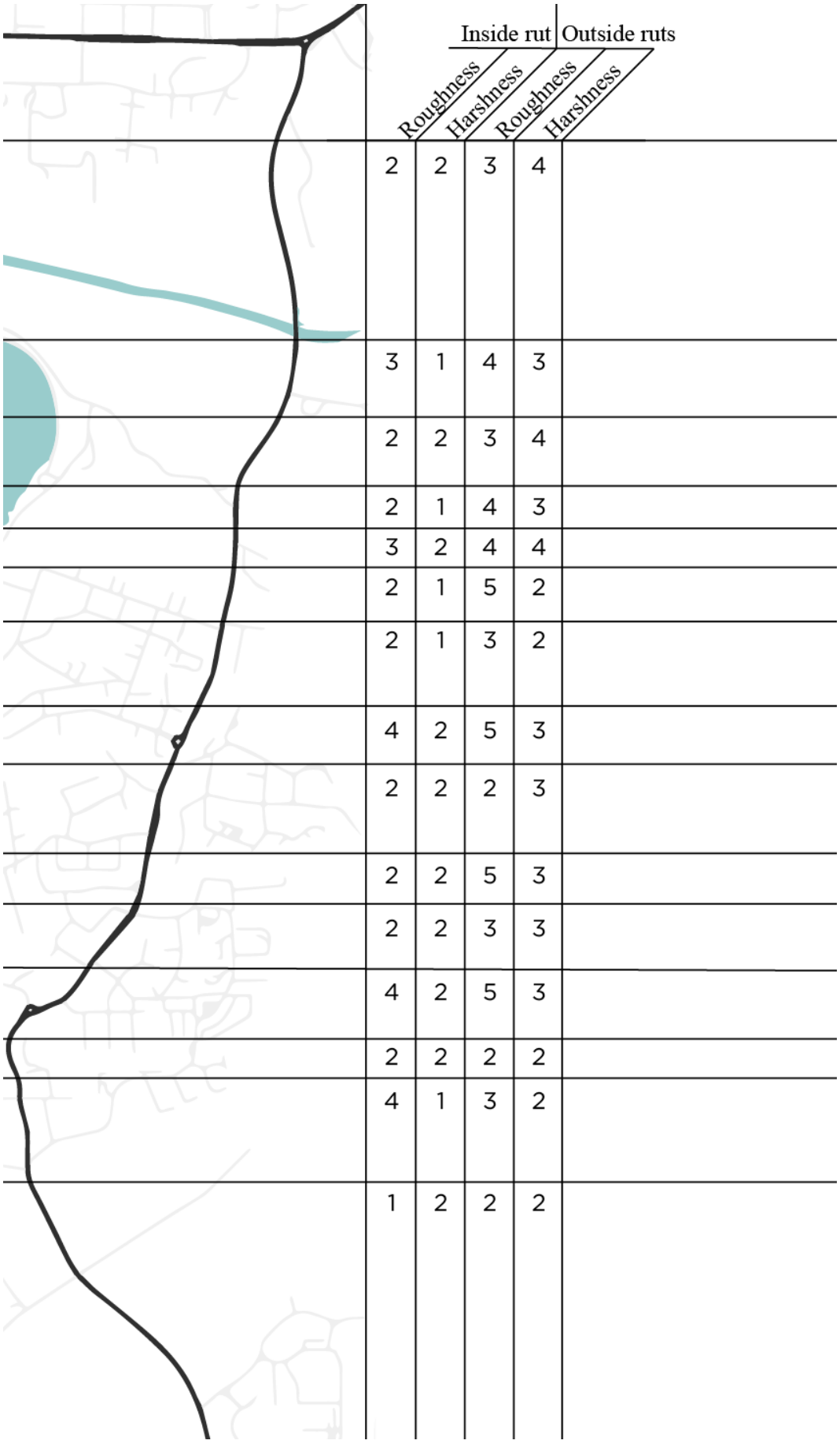

Figure 19: Map of the tactile surface structure index used in this study. Both roughness and harshness are measured on an index scale from 1 to 5, from smooth to rough and harsh to polished.

5 Results

5.1 Original inaccuracy source, quality and magnitude

As discussed, there are three main error sources: the algorithm, pavement colour variation and pavement structure variation. First we discuss the errors of the baseline layer thickness algorithm and then compare those results with the newer solutions. Finally we discuss the auxiliary results.

5.1.1 Pavement structure variation

The error generated by pavement structure variation stems from incongruous definitions of depth. This error is a fundamental property of optical water measurement, and essentially requires external information to eliminate. We can however create accurate approximations of its behaviour and magnitude and mitigate the extreme effects with proper averaging.

Let's recall the definitions for the centre-line-average water depth and the effective optical water depth measured by MORSE:

$$D_w(cla) = \frac{\int^A h_w(\overrightarrow{x}) - h_p(\overrightarrow{x}) d\overrightarrow{x}}{||A||}, \tag{21}$$

$$D_w(eo) = -\frac{1}{2\kappa} ln \left(\frac{\int^A e^{-2\kappa(h_w(\overrightarrow{x}) - h_p(\overrightarrow{x}))} d\overrightarrow{x}}{||A||} \right). \tag{22}$$

Now consider a road surface with the shape of a square wave with asperity height h_a and uniform base at $h = 0$, similar in structure to Figure 9. Assume also uniform water surface location h_w. Now trivially the above-aperity depth $D_w(aa) = h_w - h_a$, when $h_w \geq h_a$ and 0 elsewhere.

Similarly piece-wise, the centre-line-average depth is now defined as

$$\begin{cases} D_w(cla) = h_w/2 & h_w \leq h_a \\ D_w(cla) = h_w - h_a/2 & h_w > h_a. \end{cases} \tag{35}$$

Somewhat less trivially the effective optical depth is then defined as

$$\begin{cases} D_w(eo) = \ln\left((1 + e^{-2\kappa h_w})/2\right)/2\kappa & h_w \leq h_a \\ D_w(eo) = \ln\left((e^{-2\kappa(h_w - h_a)} + e^{-2\kappa h_w})/2\right)/2\kappa & h_w > h_a. \end{cases} \tag{36}$$

Now we can approximate $D_w(eo)$ in terms of $D_w(cla)$. Simply put, the rougher the road, the longer and further $D_w(eo)$ lags behind for the same absolute amounts of water. The left panel of Figure 20 illustrates this: the relation between the two definitions is plotted for three asperity heights, $h_a = 0$, $h_a = 1.5$ and $h_a = 2.8$ to simulate smooth, medium and rough surfaces respectively. In addition an experimentally derived effective 2κ of 1.33 is used.

To mitigate the worst errors with rough surfaces, we will here normalise the three different $D_w(eo)$ by scaling them such that the average of the three is equal to the

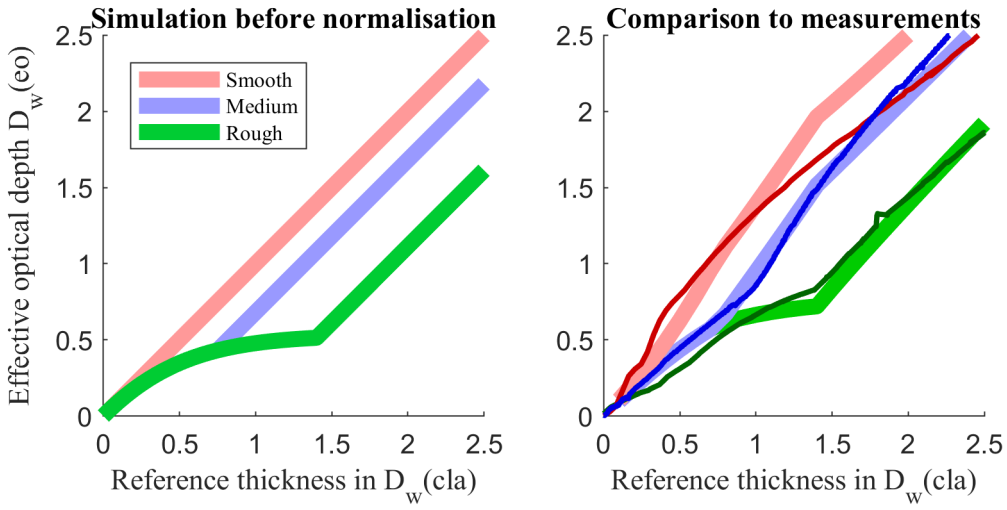

Figure 20: Theoretical and measured behaviour of the structural error are in good general agreement.

$D_w(cla)$. This way we can roughly halve the magnitude of the error. The normalised $D_w(eo)$ are presented in the right panel of Figure 20.

Most interestingly, $D_w(eo)$ produced by this very simple process offer a satisfactory match with actual measurement results: the general shape and scale of the normalised signals resembles the observed behaviour, as displayed by the darker, thinner lines. This would suggest our general understanding of the phenomenon is not far off.

According to both our measurements and the simplified simulation, at its the worst structural variation generates an error of factor 1.5, once mitigated with averaging. This is achieved by optimising the algorithm for average roughness.

As discussed, the impact of this error also depends on the application: when defining friction, the relevant thickness depends on the surface in a similar manner, meaning this behaviour could be considered desirable. Secondly, these results are congruous with the stationary sensors, such as the Vaisala DSC-211, which is good for integrating the data.

5.1.2 Pavement colour variation

The effect of pavement colour variation on the original algorithm is closely tied to the colour distribution of dry road surfaces. For the roads studied in the Helsinki general area, the baseline algorithm produces a layer thickness error of a factor of approximately 2, assuming a good choice of average dry reference. The distribution is visualised in Figure 23. This is mainly due to colour variation between different pavement types and naturally depends on the variety of pavement qualities in the measurement area. Here we will only consider the studied Helsinki general area.

One interesting finding was that of distinct pavement types presented in Figure 21. At least in the Helsinki general area the main roads fall under three main types

of road, spectrally speaking. The road types were recognised using an on-board camera, and the distinct types are on display in Figure 22.

This multimodality is further carried over to the measured layer thicknesses using the baseline algorithm, as in Figure 23. The simulated effect assumes the original measurement result to be correct, then recomputes the thicknesses using wrong dry reference information. As illustrated by the error margins in the figure, the error is consistently approximately of factor 2, naturally depending on the exact choice of dry reference, i.e. the middle point of the distribution.

This is an interesting finding in and of itself. Though there may be transitions between these poles, the poles themselves seem stable enough for use as discrete approximations of pavement colour.

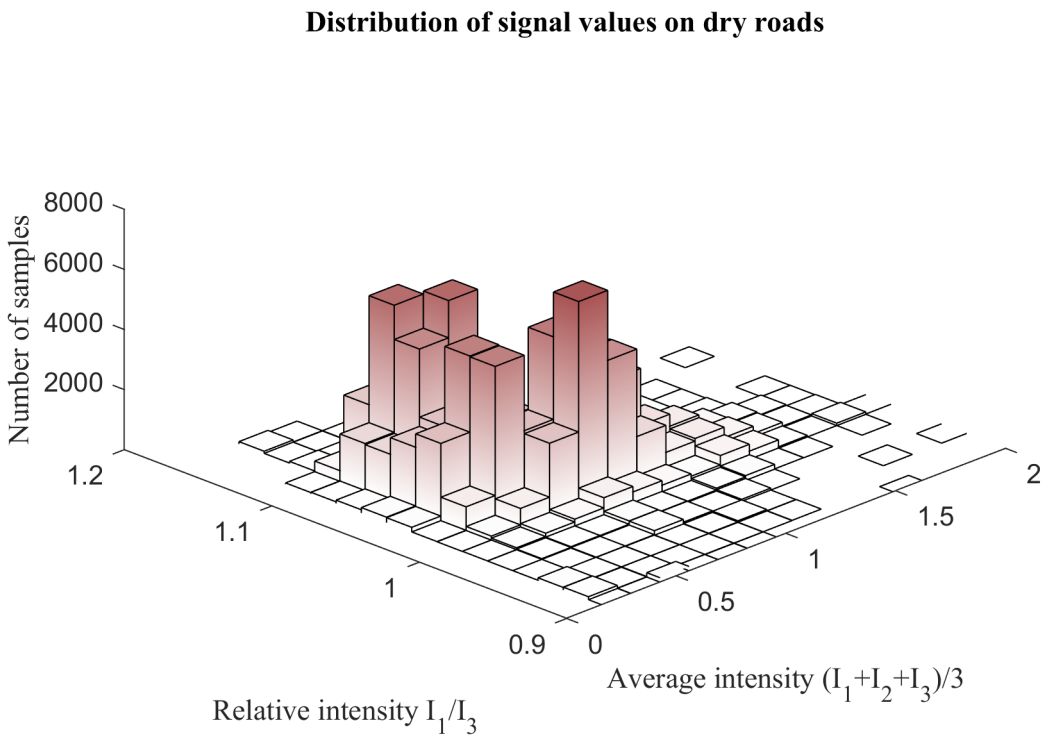

Figure 21: The spread of the dry measurement values in the Helsinki metropolitan area, plotted along the mean intensity $(I_1 + I_2 + I_3)/3$ and the spectral component I_1/I_3. The distribution shows three distinct pavement types.

Furthermore the pavement types recognised in the measurement data can be matched up

Type-internal variation produces a deviation by factor of approximately 1.1, as illustrated by Figure 23. Thus simply the correct choice of pavement type diminishes the colour variation error even in mobile measurement as long as the choice corresponds to the studied pavement.

It is also noteworthy that these two error sources operate independent of one another, but structure and surface colour themselves are often linked. Through a simple calculation we would arrive at a combined error of factor 2.25. Unfortunately

Figure 22: Examples of the three distinct pavement types recognised. On row 1 is type 1, dark, bituminous pavement. Type 2 is dark pavement with exposed aggregate, and type 3 fair, old pavement. The pavement types seem visually distinct.

the colour and roughness combine in the worst way possible: the darkest surfaces are in general the smoothest, and the fairer surfaces are the roughest. Respective examples would be slick bituminous patches and older roads with exposed aggregate. Thus these extreme errors in computed layer thickness are possible under the baseline algorithm.

5.1.3 Algorithmic error

Algorithmic error is a catch-all term for errors persistent under optimal conditions: correct dry reference, a surface of optimal roughness, and otherwise non-faulty sensor installation.

Much of the algorithmic error is subsumed by the error generated by the surface

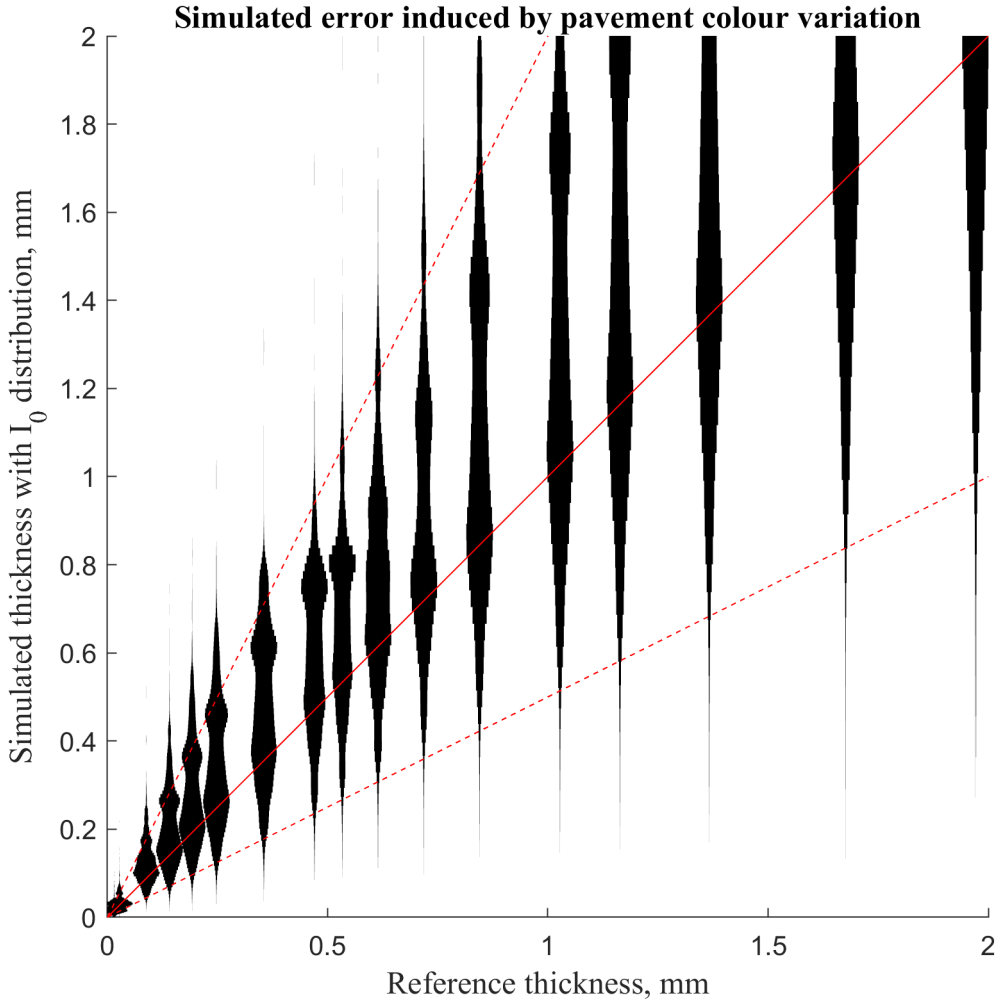

Figure 23: Simulated relative effect of pavement colour variation on the reported layer thickness values for the baseline algorithm. The profile of the markers denotes the distribution of values. The distribution is clearly multimodal.

structure: by averaging for optimal average performance, any consistent errors in the algorithm are also virtually eliminated.

More case-specific errors however persist: performance with mixed layers, response to very thin or very thick layers.

5.2 In situ roughness analysis: no results

No reasonable correlation was observed between the presented tactile surface index and the signal variation. The effects of roughness are seemingly consistently outweighed by the effects of random measurement noise and pavement colour varia-

tion: the different pavements differ more in colour than in structure. The additional fidelity achieved with square wave analysis was not sufficient to combat this.

5.3 New options for thickness algorithm

5.3.1 Pavement-agnostic lookup-table

The pavement colour variation causes primarily uniform intensity noise, as discussed in Section 2.2.1. It follows that simply studying the relative values of the signals, that is $\frac{I_1}{I_3}$ and $\frac{I_2}{I_3}$, most of the error caused by pavement colour variation can be suppressed, as the division will eliminate uniform reflectivity changes. This also effectively reduces the measurement space to two dimensions, as the third dimension $\frac{I_3}{I_3}$ contains no useful information.

This simple solution can be improved upon based on the pavement colour variation measurements discussed in Section 5.1.2. By combining non-linear preprocessing with principal component analysis 99.69 % of the pavement colour variation can be captured with the first primary component, which can then be suppressed similarly as the truly uniform intensity noise.

The resulting two-dimensional measurement space is almost completely orthogonal to the pavement colour variation, so it does not register the colour changes. The plane could be described as pavement agnostic. Once the effect of pavement colour variation has been removed, the plane is populated by projecting the reference water and ice layer measurements onto it.

A computationally low-cost lookup-table is prepared with this knowledge. The reference measurements from Section 3 are projected onto the pavement-agnostic plane, which is then evenly divided into a square mesh. A sample of the projected points is plotted in Figure 24. The average layer thickness for each face is computed, then convoluted with a Gaussian convolution matrix to ensure continuity and smoothness. For this study we used an 80-by-80 square mesh. The final measurement results can be interpolated from the LUT-values.

Figure 25 illustrates the general performance of the LUT once assembled. Most notably there is minimal colour variation error: the algorithm is largely pavement-agnostic, as discussed. The great improvements in mix-layer measurement might be partially over-fitting of the LUT, as there were only a few measurement series of mixed water-ice layers. The general performance for both ice and water measurement is slightly worse than the baseline algorithm: removing the susceptibility to pavement colour variation also limits the sensitivity to layer thickness variation.

There are a couple of algorithmic error sources for this solution. The method fares poorly with very thin layers, as it fails to capture wetting induced reflectance depression. In the projected plane the effect overlaps itself, rendering accurate measurement thereof virtually impossible. The ill effects of the overlap could be mitigated by subdividing the LUT mesh near dry values, but the overlapping part itself remains problematic.

The LUT is also very sensitive to base measurement noise in the signal values: should the noise level higher or lower than in the data be used to construct the LUT,

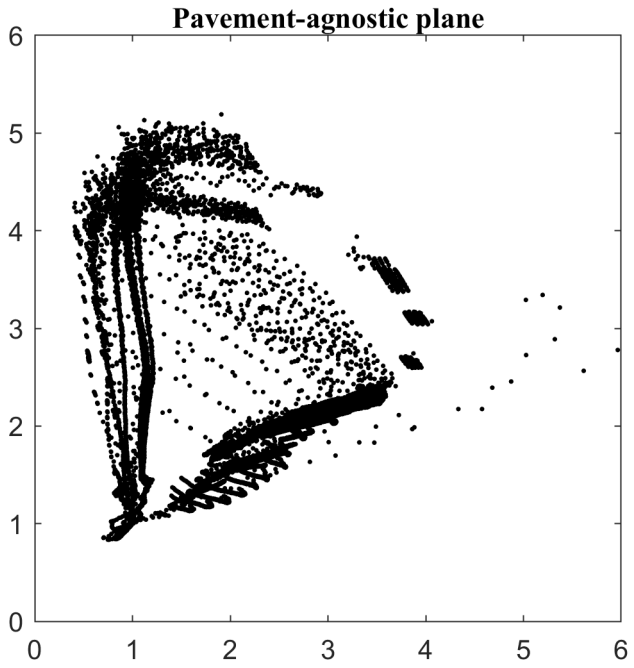

Figure 24: Logarithm of the reference measurements projected into the pavement-agnostic plane. The vertical line corresponds with water measurements and the diagonal line with ice measurements, while the points in between are mixed layers. The curve near value 5 is due to measurement noise. The axes are arbitrary axes, chosen from the plane defined by the first principal component such that all data are in the positive quarter, and increasing values correspond to increasing layer thickness.

the results for thicker layers may be wildly inaccurate.

Lastly the LUT performs poorly with 'frosty' white ice surfaces. While is outperforms the baseline algorithm, frosty ice surfaces tend to be classified as partly water, and feature substantial drops in measured ice thicknesses.

Maintaining and updating the LUT is extremely simple: the values of any cell in the mesh can be manually set to correspond to any given value. The values can be either results from further laboratory measurements or ad hoc -values. Thus any consistent error in the LUT is simple and easy to fix, provided the error can be duplicated in the laboratory, and is not a direct result from the restrictions of the algorithm previously discussed.

5.3.2 Physical model

The physical model discussed in Section 4.4 did not fare as well. Its performance was measured only with the tests for water. Since the performance with them was deemed insufficient, the model was not extended to ice surfaces.

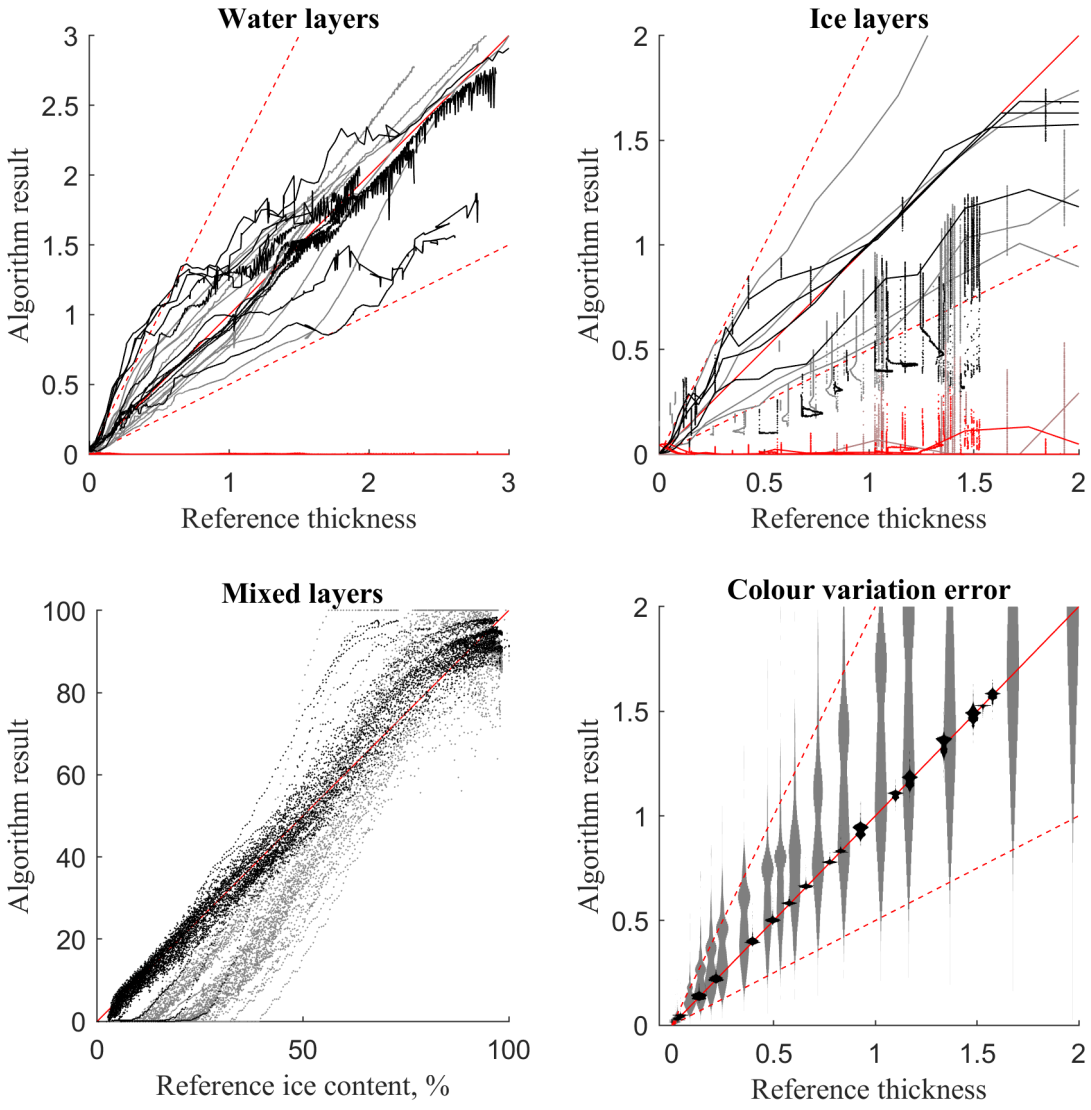

Figure 25: Performance of the pavement-agnostic lookup-table. The performance of the new algorithm (black) is compared with that of the old one (grey). Red ticks denote false readings of water when only ice is present and vice versa, fairer colour once again reserved for the old algorithm.

If we once again recall the equation we used to compute the thicknesses:

$$min_{n,l}\left(\sum_{i=1}^{3}\left(I_{0i_n}e^{-2l\kappa_i\rho(l)}D(l)-I_i\right)^2\right) \tag{28}$$

.

As the first attempts with this formula proved highly unstable, some slight modifications to the parameters were made, while the physical basis of the model remained the same.

As an attempt to better capture the pavement structure we changed $\rho(L)$ from

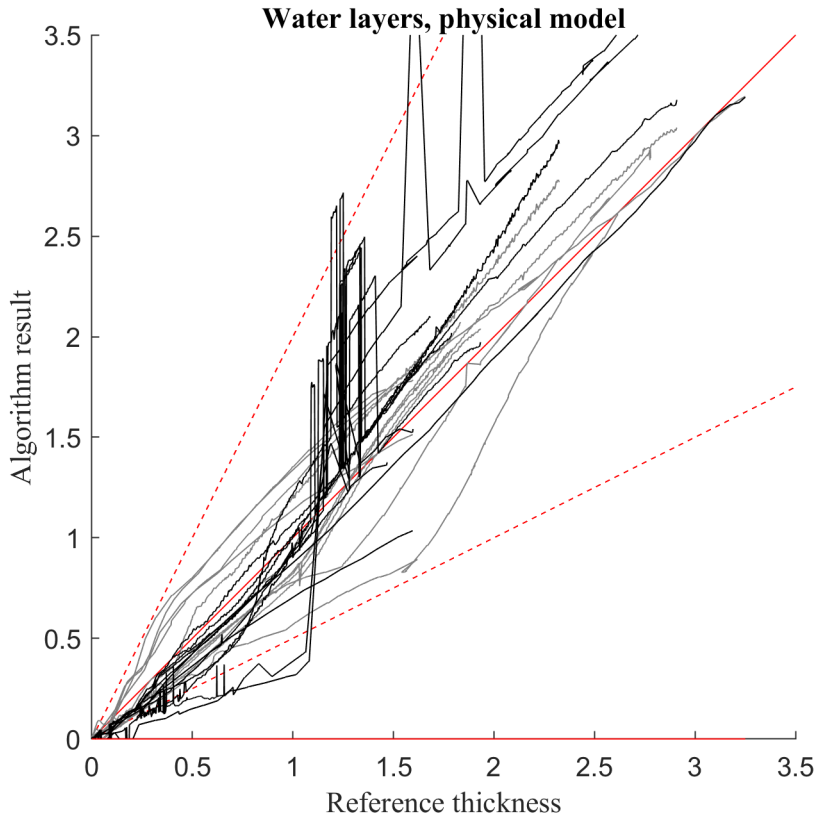

Figure 26: Water layer performance for the physical model struggles with high asperity samples and 1.3mm depth.

the basic square wave to a sawtooth wave with intervals. Interestingly, this 2-dimensional waveform corresponds with evenly spaced hemispheres in three dimensions, i.e. the height distribution of a hemisphere is linear. This is perhaps a more accurate approximation of the pavement surface, specifically the typical abstraction of asperities. By integrating the depth with the correct extinction coefficient for each wavelength we can more accurately approximate the absorption.

Secondly, a constant parameter I_b was added to represent the lowest measurable intensity: even when measuring an effectively bottomless container of water, a small non-zero intensity is attained, as the light bounces off of the water surface. This was approximated as roughly one thousandth of the original intensity I_{0i} for each wavelength. By accounting for this slight inaccuracy we can more accurately report thick layers.

However,with these adjustments the model still struggles with just the water layers, even with the prior knowledge of absence of ice. The most visible issues are under and subsequently overestimating water layers on high asperity surfaces, and notable unwieldiness in the 1.3 mm region, as is apparent from Figure 26.

The performance is actually quite good for the medium and low asperity samples,

outperforming both the baseline model and the model presented in the previous section: the method shows some promise. It however does not capture the high asperity behaviour.

Since the model can't accurately backwards compute just the water layers, it will definitely also fail when further optimisation parameters are added, making the task increasingly more complex. Thus the physical mode was deemed unsuccessful, and not implemented further.

6 Discussion

This work set out to better understand and develop mobile road weather measurement. In retrospect the practical part of the work was larger than expected, as the field has not yet fully matured: there is no wide consensus on the best practices on water layer measurement on pavement surfaces.

The basic physics discussed form a solid foundation for future discussion on the subject, enabling more in depth understanding of e.g. the importance of pavement structure for optical road weather measurement. This is a benefit for the entire field of commercial road weather measurement.

6.1 Pavement-agnostic model

The pavement agnostic look-up-table achieved its goals: it is very robust against pavement colour variation with little to no compromise required on either best case performance or structure variation. Due to the dimensionality reduction the table is also small enough to fit in memory and light to operate.

6.1.1 Limitations

The model fares poorly with different pavement structures, even more so than the baseline model. This is somewhat expected, as removing one dimension does remove a sizeable amount of information.

There may also be an additional cost in robustness to other error sources. The model might be more susceptible to error due to e.g. window dirtiness. In general it is more vulnerable to spectral error while mostly ignoring intensity error. For the specific application of mobile measurement this is however likely an acceptable trade-off.

6.2 Shortcomings the physical model

Despite our best efforts the physical model does not ultimately capture the behaviour of the signals. The performance is however still remarkable: for the low-to-medium asperity size the model performs quite well, suggesting the absorption equations do hold up rather well. While the model itself might not be suitable for the application, it does shed light on the phenomenon, increasing our general understanding.

Specifically, its failures pose an interesting question: what phenomena are we missing? The current known unknowns might pose interesting questions for future research. Since the in-depth study of these phenomena is out of the scope of this work, we naturally can't conclude that they are the reason behind the poor performance.

6.2.1 Co-dependent parameters

We did not account for wavelength-dependency in the wetting induced reflectance depression parameter $D(l)$, or its relation to roughness. While Section 5.1.1 pre-

sented some results, the simplified square-wave model did not capture the full truth: the link between roughness, reflectance depression and spectral variation is more complex than what we hoped for: especially the roughness and signal depression seem to interact in ways our model did not capture. Thus the minimising equation has a strong tendency for error for different types of pavement – not succeeding in its sole task of capturing this difference.

A link between roughness and wetting is also easy to imagine: it might take a different amount of water to wet a rougher surface with more surface area. Wetting seemed to differ between the samples studied, but as we only housed a handful of samples, implementing a co-dependency would have been rather irresponsible: at this point we can claim no real understanding of the phenomenon in road context. Finding any trend in the few samples we had would be highly vulnerable to overfitting.

Secondly, we know for certain that the wetting induced signal depression is not wavelength-invariant, as the model assumed. As of now we however do not have a resounding explanation for the spectral changes observed during wetting but before layer build-up, so no feature could be implemented in the physical model. The basic theory discussed in Section 2.2.3 does roughly explain the scale of the overall signal decrease, but does not account for the scale of the spectral component. Even though the Fresnel equation features slight wavelength dependence, as the refraction indices vary for different wavelengths, the effect is not as large as that observed.

6.2.2 Pavement structure oversimplified

Similarly suspect is the simplification used for pavement structure variation. We used simply linear scaling of the distribution, i.e. rougher pavement was modelled just as scaled smoother pavement. In reality, pavements feature differing size distributions, and a single scaling parameter for average asperity size is not sufficient as such.

Most likely by making the length of the saw-tooth tail, i.e. the asperity density, and the asperity height adjustable the model could more accurately capture rougher pavements. The asperities on rougher pavements are wider than they are tall, and are relatively more densely packed than those on smoother pavements. This would add two additional parameters, which would likely over-complicate the computation. Another solution would be to include a roughness-harshness model with two different asperity sizes interacting. We could link these parameters with the different pavement types identified, as dark pavements often feature smaller asperities and the fairer pavements larger, more polished asperities. This way we could avoid increasing the number of optimisation parameters and the complexity of the problem.

Pairing the pavement colour profiles with the structure variables will however require more measurements with numerous samples. As we were in this work studying but a handful of samples in the laboratory, assigning structural values would be highly vulnerable to over-fitting, once again.

If allowed to speculate, this could be identified as the most likely reason for the

poor performance of the physical model, as it specifically struggled with the asperity size.

6.2.3 More complex model

By updating the equation to account for dependencies on interaction, wavelength and pavement-type specific roughness functions, we would get a more complex equation

$$min_{n,l}\left(\sum_{i=1}^{3}\left(I_{0i_n}e^{-2l\kappa_i\rho_n(l,i)}D(l,i,\rho)-I_i\right)^2\right), \tag{37}$$

which might result in more accurate road state measurement after sufficient study. In this work we have however not studied the spectral component of either of the phenomena, so studying this model is decidedly out of the scope of this work.

The complexity of the equation also naturally increases with additional parameters. Our understanding of the issue at the time of writing is not sufficient to account for these parameters and their interaction in a robust, physical manner.

6.2.4 Computational costliness

The current version of the physical algorithm uses the discussed Nelder-Mead algorithm to find a local minimum for the optimisation. This requires numerous iterations and is ultimately rather cumbersome to compute, especially if the different pavement qualities were added, multiplying the required computation.

The cost could be alleviated by using gradient descent methods. The functions used are all differentiable in closed form, so more efficient methods are available. However as the model was not finalised, these options were not studied. Due to their iterative nature, they might still prove too cumbersome for the mobile application, especially once the number of parameters increases.

6.3 In situ roughness analysis

As discussed, the changes in pavement colour outweigh any effect the changing measurement distance has: the pavement structure and colour are codependent always change together, contaminating any structure measurement. Thus it most likely is not possible to directly measure pavement roughness from the measurement signal.

The square wave analysis did ultimately little to help this, as the issue was not the signal-to-noise-ratio of our measurement.

Indirect approximation might however be possible: the structure and coloration correlate. By using the pavement-agnostic dimensions to compute the layer thicknesses, it is possible to approximate the effect the layer in question would have on the third dimension, now discarded. Through backwards-computation one could then arrive at an estimate of the dry colour of the pavement, which correlates with the roughness, as presented in Figure 22.

This is however a data heavy process, as one would have to quantify the link between pavement colour and structure. Our current set of laboratory samples is woefully insufficient for such a task, but they are the only samples we have reliable roughness estimates on currently.

6.4 High quality reference measurements

Somewhat surprisingly the advances in water layer measurement on road surfaces might be the most valuable result of this work. The current methods used are varied and often ill-defined or ill-suited for the application: even modern research sacrifices little thought to rigorous definition of layer thickness. The combination of dual-reference measurement and passive layer manipulation through evaporation offers remarkably accurate reference data though it may not be suited for all measurement situations. The definition of thickness need not be strictly defined when using this measurement setup: as one has both the information for $D_w(aa)$ and $D_w(ie)$, either one or any combination of them can be used.

Secondly the importance of thin layers is seemingly oft overlooked: The effect a 0.1 mm layer has on the road surface is counter-intuitive. Especially when defining depth as the above-asperity depth, a road surface with 0.1 mm of water is basically flooding. Especially in the case of ice, the thickness is rather unimportant: even a thin layer of wet, slippery ice can cause near complete loss of friction [10].

The reason for ignoring the thinner layers could be both due to intuition and practicality. As one would intuitively expect their effect on friction on to be negligible, and they are very hard to produce through active manipulation, leaving them out is a compelling option.

6.5 Future research required in pavement structure

As our understanding of the effects of pavement structure progresses, we can achieve ever more accurate road weather information. The structure is the largest remaining source of error, so tackling it is the logical next step.

A competitor of Vaisala in the road measurement field previously claimed to have developed technology that "automatically adjusts the recording of the conditions to the surface structure", but there is no more mention of it in the manual [15]. This may hint at a fundamental scope problem in pavement measurement: globally there are a vast number of different types of pavements, and correcting for approximated pavement quality may actually result in less reliable measurements. As these devices are used to prevent loss of life, it follows that unreliable measurements may risk lives. This is a reason why we were reluctant to draw roughness conclusions from our relatively small number of pavement samples: not only would the result generalise poorly, but it could endanger lives doing so.

Better understanding the effect of pavement structure on optical measurement could be a fruitful subject for future research even outside the corporate domain.

7 Conclusion

The beginning and basis of this work was the design of the laboratory measurements of layer thickness. The work done in the laboratory proved to be more valuable than anticipated: we were able to link and discuss the different definitions of thickness, and produce high-quality reference measurements. The methods presented are of value to future research in the field, useful for standardising and comparing optical road measurement performance.

The simple pavement-agnostic LUT model presented leverages the measurements both in and outside of the laboratory to a great degree. The model successfully eliminates the effect of road colour changes in mobile measurement with acceptable trade-offs in performance when compared with the baseline model. The model is also computationally light enough to be ran in the rapid measurement cycle of the MORSE sensor.

In addition to practical measurements, we also presented a simple physical model of the optics of road weather measurement, going over the basics physics of the situation. This has both deepened our understanding on the subject and led to the backwards computation physical layer thickness model.

The physical layer thickness model however struggles with surface structure, suggesting or understanding on the subject is lacking. Similarly the on board structure analysis bore no fruit, as analysing the surface structure proved itself an issue more complex than expected. This raises a call for future research into the surface structure. By developing heuristics for approximating height distribution of different pavement qualities and approximating their effect on the optical road weather measurements we could achieve better performance in any and all of the discussed layer thickness models.

References

[1] Minh-Tan Do et al. “Influence of Thin Water Film on Skid Resistance”. In: *Journal of Traffic and Transportation Engineering* 2 (June 2014), pp. 36–44.

[2] Alan Dunford. “Friction and the texture of aggregate particles used in the road surface course”. July 2013. URL: http://eprints.nottingham.ac.uk/13412/.

[3] George M. Hale and Marvin R. Querry. “Optical Constants of Water in the 200 nm to 200 µm Wavelength Region”. In: *Appl. Opt.* 12.3 (Mar. 1973), pp. 555–563. URL: http://ao.osa.org/abstract.cfm?URI=ao-12-3-555.

[4] Kazuo Hisatake, Satoko Tanaka, and Youko Aizawa. “Evaporation rate of water in a vessel”. In: *Journal of Applied Physics* 73.11 (1993), pp. 7395–7401. eprint: https://doi.org/10.1063/1.354031.

[5] T. Kohonen, M. R. Schroeder, and T. S. Huang, eds. *Self-Organizing Maps*. 3rd. Berlin, Heidelberg: Springer-Verlag, 2001. ISBN: 3540679219.

[6] B. T. Kulakowski and D. W Harwood. “Effect of Water-Film Thickness on Tire-Pavement Friction.” In: *Surface Characteristics of Roadways : International Research and Technologies, ASTM STP 1031*. Ed. by W. E. Meyer and J. Reichter. Philadelphia: American Society for Testing and Materials, 1990, pp. 50–60.

[7] John Lekner and Michael C. Dorf. “Why some things are darker when wet”. In: *Appl. Opt.* 27.7 (Apr. 1988), pp. 1278–1280. URL: http://ao.osa.org/abstract.cfm?URI=ao-27-7-1278.

[8] Åsa Laurell Lyne et al. “Characterization of stripping properties of stone material in asphalt”. In: *Materials and Structures* 46.1 (Jan. 2013), pp. 47–61. ISSN: 1871-6873. URL: https://doi.org/10.1617/s11527-012-9882-6.

[9] William P. Mahoney and James M. O’Sullivan. “Realizing the Potential of Vehicle-Based Observations”. In: *Bulletin of the American Meteorological Society* 94.7 (2013), pp. 1007–1018. eprint: https://doi.org/10.1175/BAMS-D-12-00044.1.

[10] Lasse Makkonen and Maria Tikanmäki. “Modeling the friction of ice”. In: *Cold Regions Science and Technology* 102 (June 2014), pp. 84–93.

[11] Behrouz Mataei et al. “Pavement Friction and Skid Resistance Measurement Methods: A Literature Review”. In: *Open Journal of Civil Engineering* 06 (Jan. 2016), pp. 537–565.

[12] Lina Nordin et al. “Road Surface Wetness Variations: Measurements and Effects for Winter Road Maintenance”. In: *Journal of Transportation Engineering* 139.8 (2013), pp. 787–796. eprint: https://ascelibrary.org/doi/pdf/10.1061/\%28ASCE\%29TE.1943-5436.0000546.

[13] Kent F. Palmer and Dudley Williams. “Optical properties of water in the near infrared∗”. In: *J. Opt. Soc. Am.* 64.8 (Aug. 1974), pp. 1107–1110. URL: http://www.osapublishing.org/abstract.cfm?URI=josa-64-8-1107.

[14] Olympia Panagouli and Alexandros Kokkalis. "Skid resistance and fractal structure of pavement surface". In: *Chaos, Solitons & Fractals* 9 (Mar. 1998), pp. 493–505.

[15] Lufft Mess- und Regeltechnik GmbH. *MARWIS-UMB / STARWIS-UMB Operating Manual V 3.0*. 2017. URL: https://www.lufft.com/download/manual-lufft-marwis-starwis-en/.

[16] Osvaldo Skliar, Ricardo E. Monge, and Sherry Gapper. "A New Method for Signal and Image Analysis: The Square Wave Method". In: *CoRR* abs/1501.00680 (2015). arXiv: 1501.00680.

[17] Athanasios Theofilatos and George Yannis. "A review of the effect of traffic and weather characteristics on road safety." In: *Accident; analysis and prevention* 72 (2014), pp. 244–56.

[18] Andreas Ueckermann et al. "Calculation of skid resistance from texture measurements". In: *Journal of Traffic and Transportation Engineering (English Edition)* 19 (Feb. 2015), pp. 3–16.

[19] Vaisala. *Remote Road Surface State Sensor DSC111*. 2014. URL: https://www.vaisala.com/sites/default/files/documents/DSC111-Datasheet-B210470EN-C.pdf.

[20] A. G. Veith. "Tires - Roads - Rainfall - Vehicles: The Traction Connection". In: *Frictional Interaction of Tire and Pavement, ASTM STP 793*. Ed. by W. E. Meyer and J. D. Walter. American Society for Testing and Materials, 1983, pp. 3–40.

[21] Sossio Vergara. "A Synthesizer based on square waves". In: *CoRR* abs/0804.3241 (2008). arXiv: 0804.3241.

[22] Sossio Vergara. "Nonorthogonal bases and phase decomposition: Properties and applications". In: *Digital Signal Processing* 24 (Jan. 2014), pp. 223–230.

[23] Stephen G. Warren and Richard E. Brandt. "Optical constants of ice from the ultraviolet to the microwave: A revised compilation". In: *Journal of Geophysical Research: Atmospheres* 113.D14 (2008). eprint: https://agupubs.onlinelibrary.wiley.com/doi/pdf/10.1029/2007JD009744.

[24] Yuchuan Wei. "Frequency analysis based on general periodic functions". In: *Journal of Mathematical Physics* 40.7 (1999), pp. 3654–3684. eprint: https://doi.org/10.1063/1.532915.

[25] Yuchuan Wei and Nanxian Chen. "Square wave analysis". In: *Journal of Mathematical Physics* 39.8 (1998), pp. 4226–4245. eprint: https://doi.org/10.1063/1.532493.